RSC Advances

ROYAL SOCIETY OF CHEMISTRY

www.rsc.org/advances

Proposed kinetic mechanism for *Mt*IMPDH in the presence of K^+.

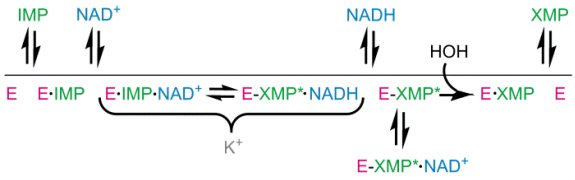

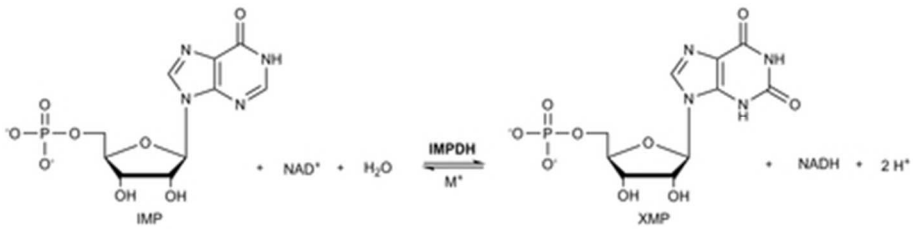

38x9mm (300 x 300 DPI)

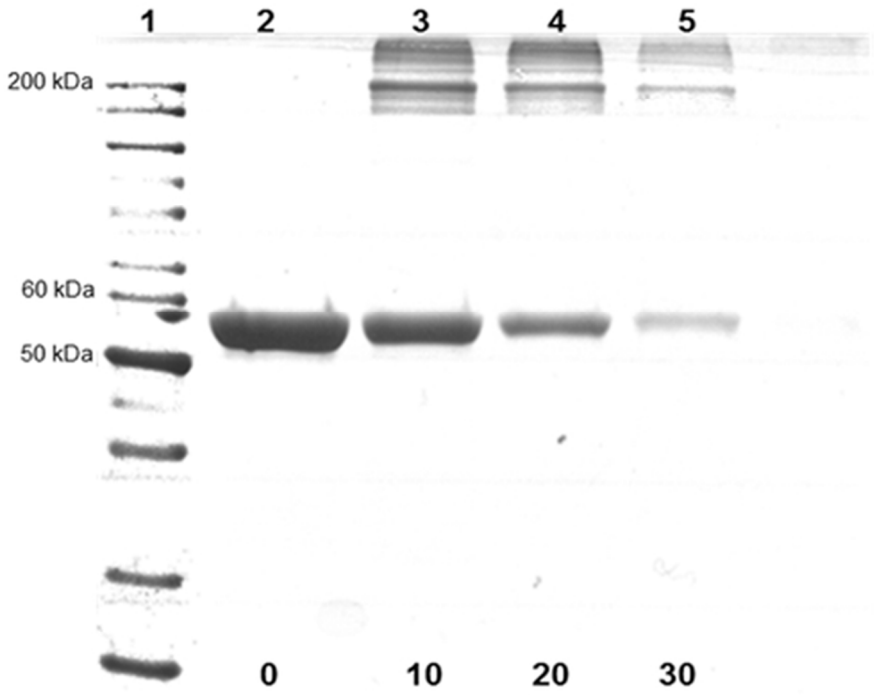

61x46mm (300 x 300 DPI)

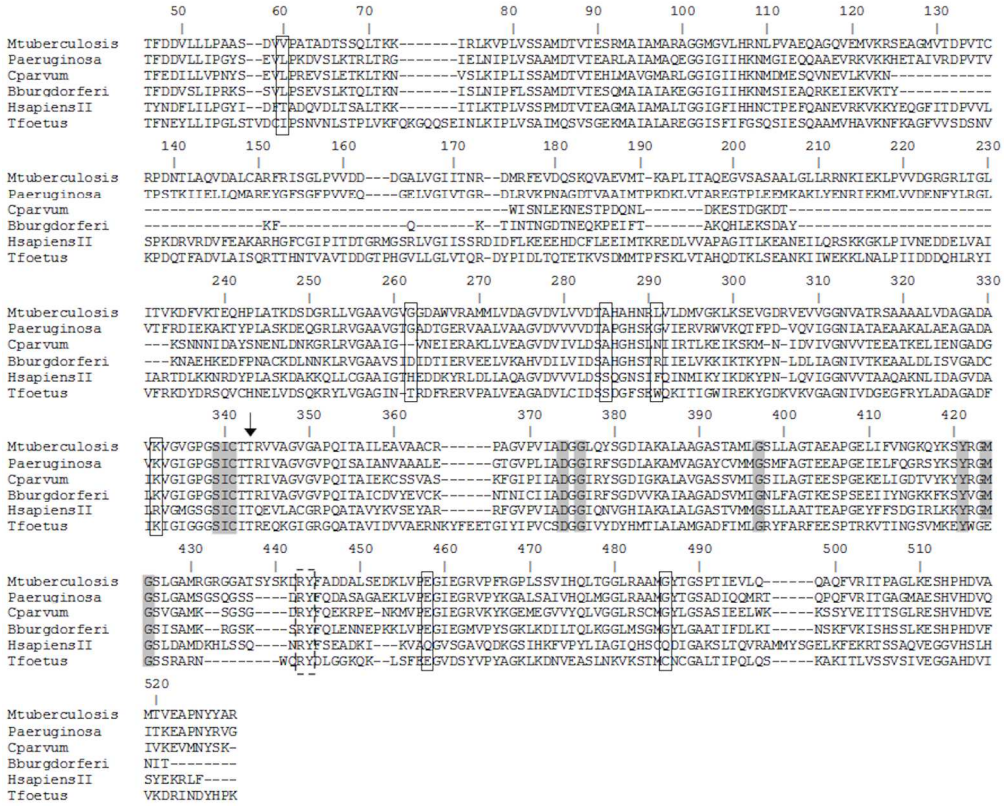

160x129mm (300 x 300 DPI)

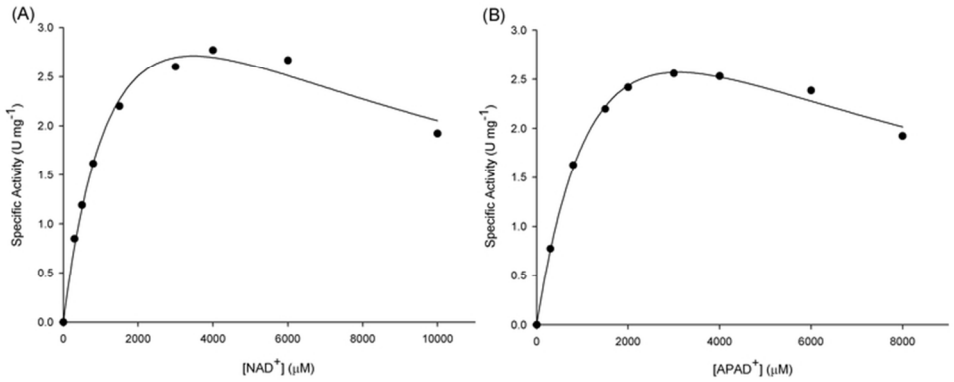

70x29mm (300 x 300 DPI)

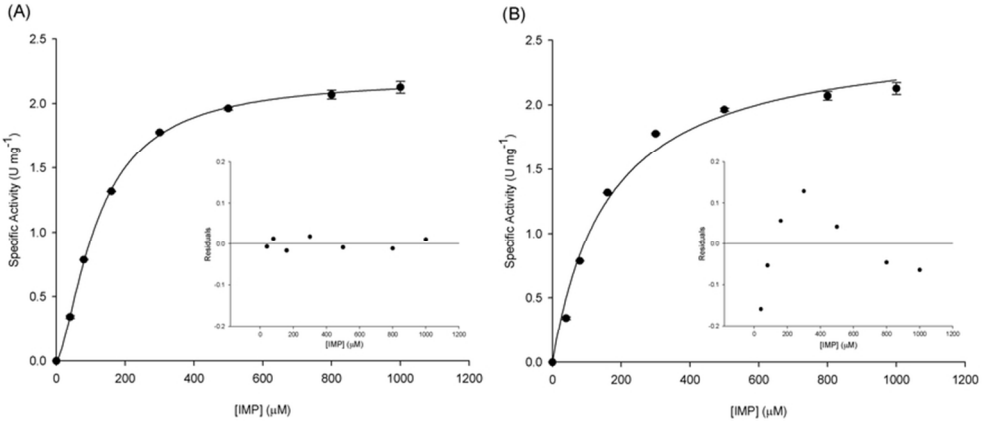

75x33mm (300 x 300 DPI)

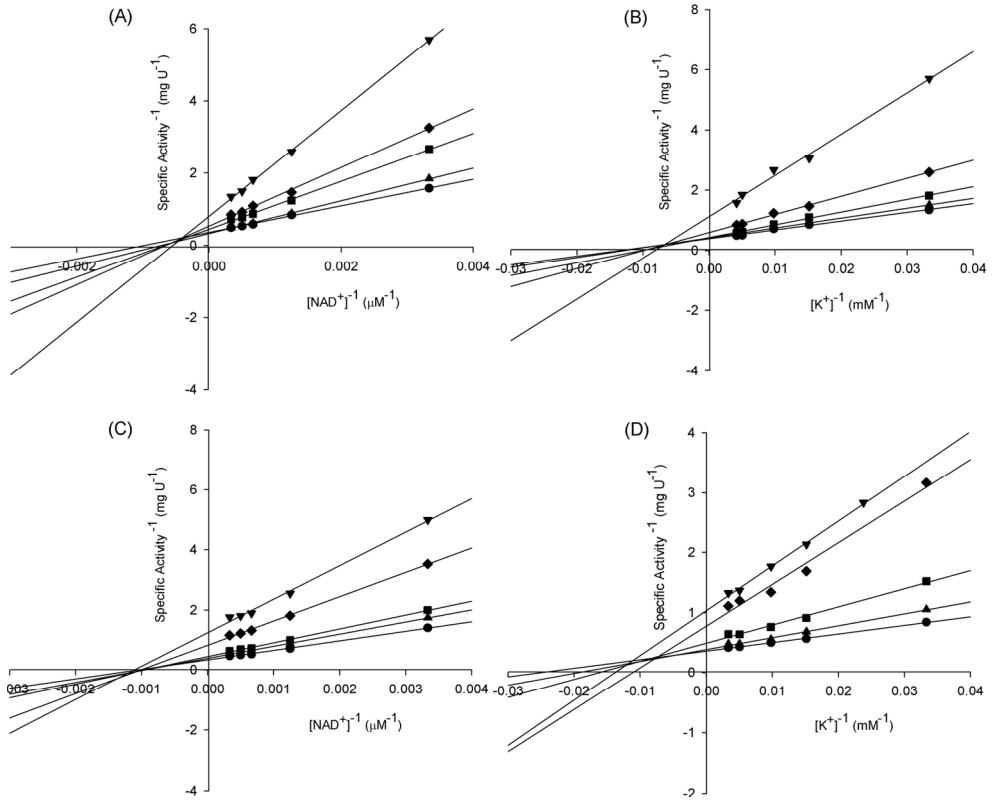

146x124mm (300 x 300 DPI)

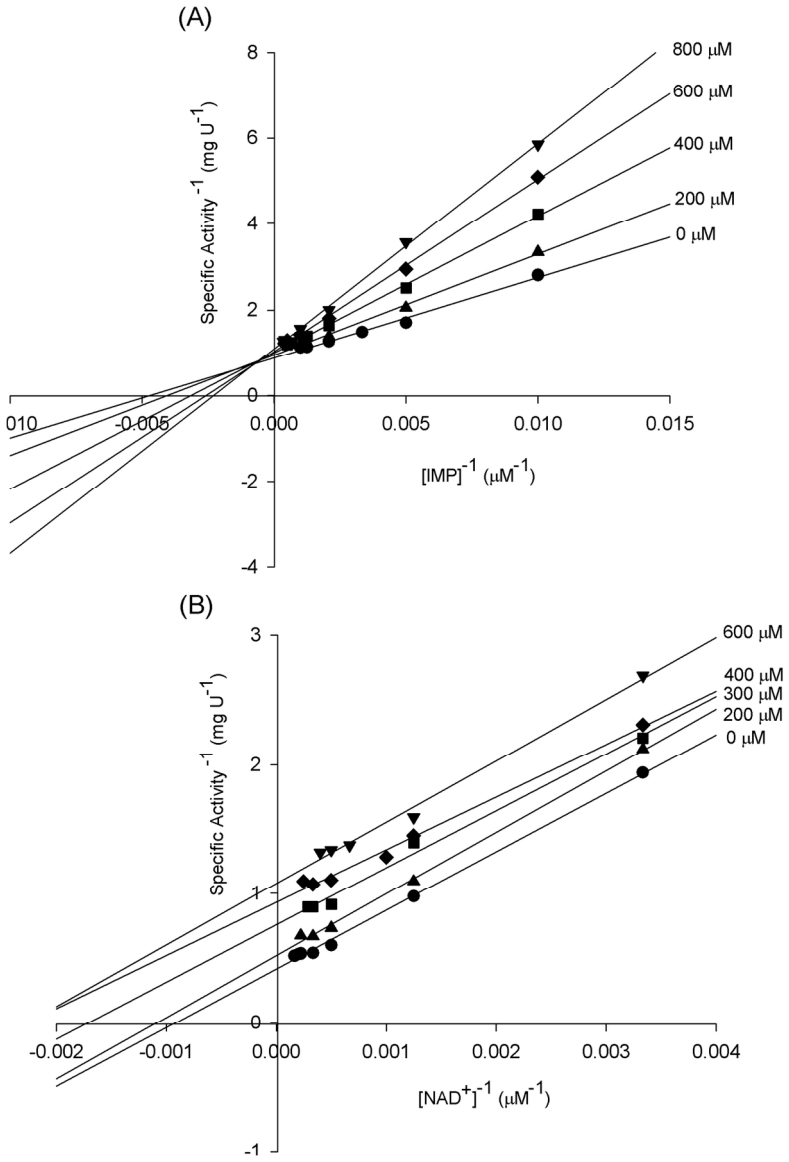

125x189mm (300 x 300 DPI)

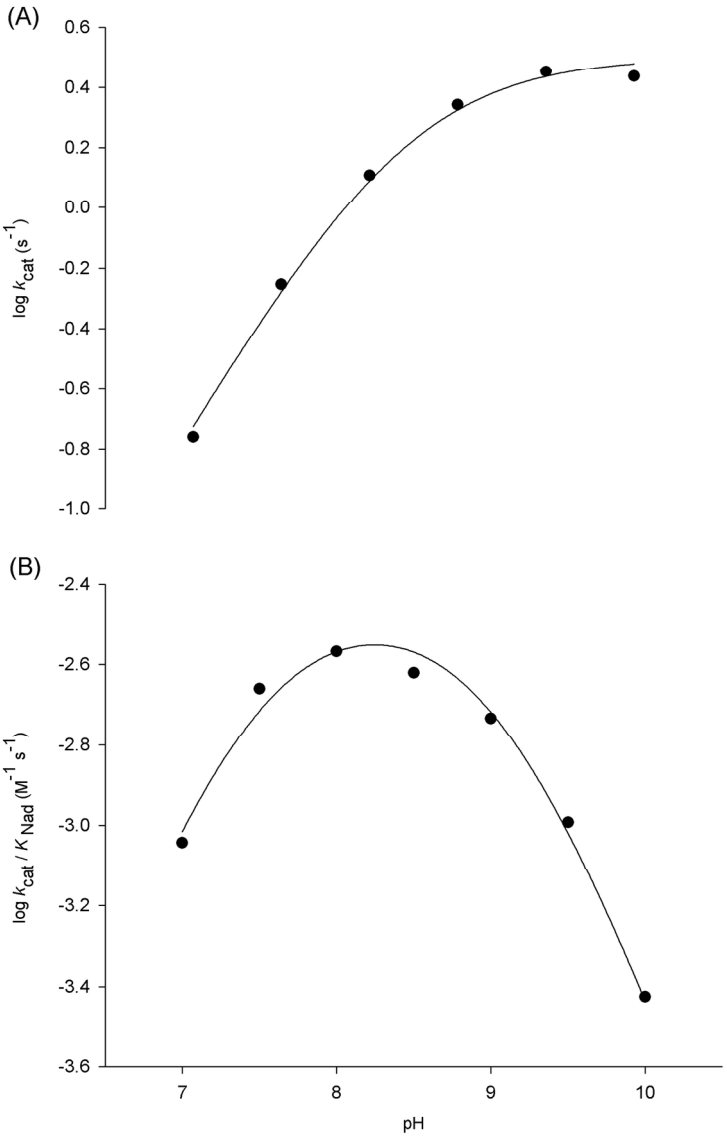

128x200mm (300 x 300 DPI)

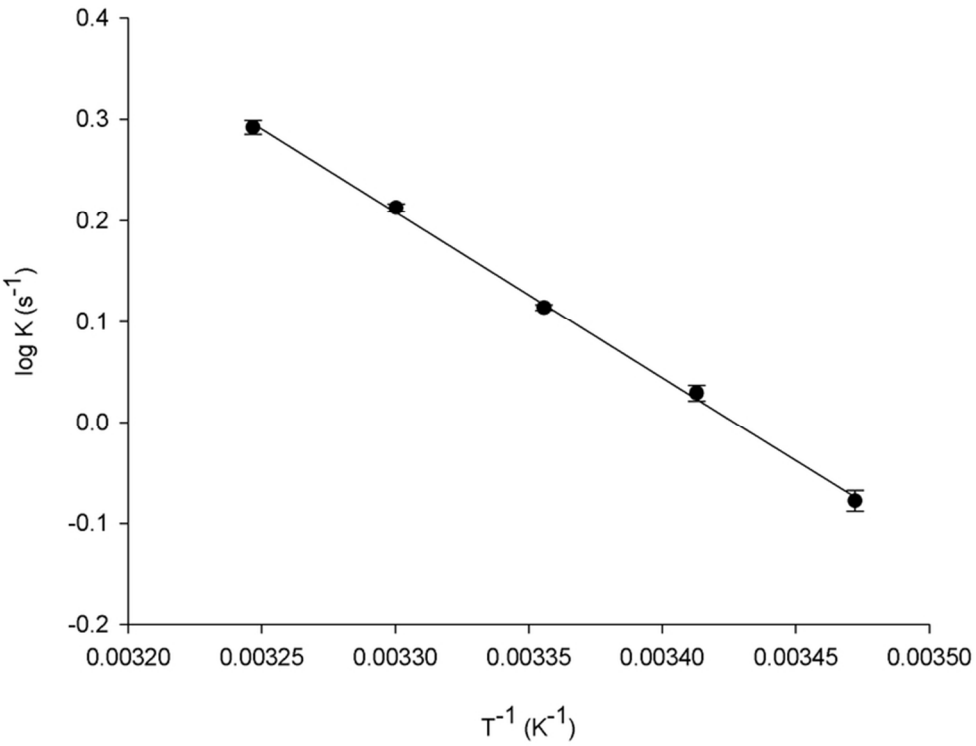

70x60mm (300 x 300 DPI)

Biochemical characterization of *Mycobacterium tuberculosis* IMP dehydrogenase: kinetic mechanism, metal activation and evidence of a cooperative system

Diana Carolina Rostirolla[ab], Thiago Milech de Assunção[c], Cristiano Valim Bizarro[a], Luiz Augusto Basso[ab*] and Diogenes Santiago Santos[ab*]

[a]Centro de Pesquisas em Biologia Molecular e Funcional (CPBMF), Instituto Nacional de Ciência e Tecnologia em Tuberculose (INCT-TB), Pontifícia Universidade Católica do Rio Grande do Sul (PUCRS), 6681/92-A Av. Ipiranga, 90619-900, Porto Alegre, RS, Brazil.

[b]Programa de Pós-Graduação em Medicina e Ciências da Saúde, PUCRS, Av. Ipiranga 6681, Porto Alegre, RS, Brazil.

[c]Gastroenterology Research Unit, Mayo Clinic, Rochester, MN 55905, USA.

*Corresponding authors: Luiz A. Basso or Diogenes S. Santos
Av. Ipiranga 6681 – Tecnopuc – Prédio 92A, ZIP CODE 90619-900, Porto Alegre, RS, Brazil. Phone/Fax: +55 51 33203629; E-mail addresses: luiz.basso@pucrs.br or diogenes@pucrs.br

Running title: Mode of action of IMP dehydrogenase from *Mycobacterium tuberculosis*.

Summary

Enzymes from the nucleotide biosynthesis pathway are potential targets for the development of novel anti-mycobacterial agents. Inosine 5'-monophosphate (IMP) dehydrogenase from *Mycobacterium tuberculosis* (*Mt*IMPDH) catalyzes the oxidation of IMP to XMP, with concomitant conversion of NAD^+ to NADH. In the present work, the *guaB2*-encoded *Mt*IMPDH has been cloned, expressed and purified to homogeneity. The recombinant *Mt*IMPDH has a subunit molecular mass of 54,775 Da, and Inductively Coupled Plasma Optical Emission Spectroscopy and Flame Atomic Absorption Spectroscopy identified a K^+ ion per subunit. Glutaraldehyde cross-linking data suggest that *Mt*IMPDH predominates as a tetramer. Steady-state kinetics showed that *Mt*IMPDH optimal activity is dependent on the presence of a monovalent cation, mainly K^+. Initial velocity and product inhibition patterns suggest a steady-state ordered Bi Bi kinetic mechanism in which IMP binds first followed by NAD^+, and product release is ordered. Hydride transfer appears not to be rate-limiting. The pH-rate profile indicates one deprotonated group essential for catalysis and that groups with p*K* values of 7.5 and 9.0 are important for NAD^+ binding. Temperature studies were employed to determine the activation energy of the reaction. The data presented here are discussed in light of the kinetic and structural information available for IMPDHs.

Keywords: nucleotide biosynthesis; inosine 5'-monophosphate dehydrogenase; steady-state kinetics; monovalent cation; substrate inhibition; pH-rate profile.

Introduction

In 1993, the World Health Organization (WHO) declared tuberculosis (TB) a global public health emergency and, although control efforts are making an impact on the incidence of TB in many areas of the world, this disease remains a serious global threat. The increasing prevalence of TB-HIV co-infection, especially in the African region,[1] and the emergence of multi and extensively drug-resistant (MDR-TB and XDR-TB, respectively) strains of *Mycobacterium tuberculosis*[2,3] have highlighted the need for new control measures. Novel regimens to treat all forms of TB are emerging, but in spite of this, the current TB treatment options are suboptimal and new anti-TB drugs are needed.[4,5] In order to find and validate new molecular targets for drug discovery, it is crucial to understand the biochemistry of mycobacteria,[6] which thereby prompts basic research on *M. tuberculosis* metabolism as a worth pursuing effort. Advances in the identification of new TB drug targets have been driven by the availability of the genome sequence of *M. tuberculosis* H37Rv,[7] and include elucidation of the role played by proteins of essential biochemical pathways for mycobacterial growth.[8]

Inosine 5'-monophosphate (IMP) dehydrogenase (IMPDH) represents an interesting target for the above mentioned efforts. IMPDH (EC 1.1.1.205) is a key enzyme of the *de novo* purine nucleotide biosynthesis and has long been recognized as an important target in the quest for drugs in the antiviral, antibacterial and anticancer therapeutic areas.[9-14] This enzyme catalyzes the oxidation of IMP to xanthosine 5'-monophosphate (XMP) with concomitant reduction of nicotinamide adenine dinucleotide (NAD^+) (Fig. 1), which represents a rate-limiting step in guanine nucleotide biosynthesis. XMP is then converted to guanosine 5'-monophosphate (GMP) by GMP synthetase (GMPS). Inhibition of IMPDH causes an overall reduction in guanine nucleotide pools and, as phosphoribosyl pyrophosphate (PRPP) synthetase and ribonucleotide reductase are allosterically regulated by these nucleotides, it may affect several metabolic pathways. Moreover, interruption of DNA and RNA synthesis and signal transduction results in cytotoxicity.[11,14] Although IMPDH is not generally considered an essential enzyme, since microrganisms can salvage guanine and/or xanthine *via* phophoribosyltransferase reactions, the mere presence of a salvage enzyme does not guarantee that the organism can establish an infection in the absence of IMPDH activity.[15]

The structure and biochemistry of IMPDHs have been extensively investigated.[16] Some organisms, including humans, have a double gene copy for IMPDH, denoted type I and type II, which encodes related proteins of 514 amino acid residues, showing 84% identity and similar kinetic properties.[12,17] In general, IMPDHs are homotetramers, with subunit molecular mass values of 43-58 kDa.[18-20] Each monomer has a core domain consisting of an eight-stranded α/β barrel structure which contains the active site located on the C-terminal end of the β-sheets.[21,22] In addition, IMPDHs have an evolutionary conserved subdomain composed of two cystathione β-synthase (CBS) motifs which is not required for enzymatic activity, and whose function is not yet well understood.[18,21,23,24]

All IMPDHs characterized to date are activated by K^+, although cations with similar ionic radius also activate these enzymes.[25,26] The IMPDH reaction requires two different chemical transformations, involving large conformational rearrangements in each step of the catalytic cycle.[16,27,28] In the rapid redox step, Cys331 (human type II numbering) attacks the C2 carbon atom on the IMP ring producing NADH and the covalent intermediate E-XMP*. NADH is released and a mobile flap docks in the vacant dinucleotide site, changing the enzyme into a hydrolase. E-XMP* is then hydrolyzed and XMP is released.[25,28-31]

Prokaryotic and eukaryotic IMPDHs have distinct structural features and kinetic properties, which make the development of species-selective inhibitors feasible.[15,32] Particularly, microbial IMPDHs differ from mammalian enzymes in their lower affinity for inhibitors such as mycophenolic acid (MPA) and thiazole-4-carboxamide adenine dinucleotide (TAD),[32,33] and parasite-selective inhibitors have recently been reported.[34,35] Several NAD^+/NADH binding site IMPDH inhibitors compete with the vacant dinucleotide binding site, preventing XMP release and, while the open conformation is favored in mammalian enzymes, the closed one is preferred in microbial enzymes.[25,28,31,36] In this case, the conformational equilibrium is a more important determinant of inhibitor susceptibility than the residues that contact the inhibitor.[36,37] Incidentally, Chen *et al*.[38] showed that MPA, and other active analogues against human type II IMPDH are weak inhibitors of *M. tuberculosis* IMPDH. Additionally, despite having primary sequence similarity of approximately 38%, amino acids residues which account for MPA sensitivity in human type II IMPDH,[39] are not conserved in the mycobacterial enzyme. These observations suggest that the structure

and dynamic properties of the cofactor binding site can be exploited to develop selective inhibitors.

The IMPDH from *M. tuberculosis* (*Mt*IMPDH) is encoded by the *guaB2* gene (Rv3411c) and has been proposed as a potential molecular target to inhibitors.[14,15] IMPDH activity was hypothetically attributed to the *guaB1* (Rv1843c) and *guaB3* (Rv3410c) genes.[7] However, Usha *et al*.[41] have recently demonstrated that only the *guaB2* (Rv3411c) gene encodes a functional IMPDH enzyme. The *guaB2*-gene has been predicted to be required for optimal *in vitro* growth of *M. tuberculosis* H37Rv strain by *Himar1*-based transposon mutagenesis.[42] Furthermore, a Bayesian statistical model analysis applied to deep-sequencing data for transposon-insertion libraries has supported the *guaB2* essentiality.[43] More recently, an *in silico* approach based on designed scaffolds has yielded a series of novel *Mt*IMPDH inhibitors with *in vitro* activity against *M. tuberculosis* H37Rv strains.[40]

The rational design of chemotherapeutic agents may be divided into mechanism- and structure-based designs. Augmenting the knowledge of mode of action, regulation and molecular structure of an enzyme helps lay the foundations on which to base the development of novel IMPDH inhibitors. Accordingly, here we describe cloning of the *guaB2* gene (Rv3411c) from *M. tuberculosis* H37Rv, expression and purification of recombinant *Mt*IMPDH. We also describe the activation and specificity of recombinant *Mt*IMPDH for monovalent cations (M^+). Steady-state kinetics and product inhibition studies including the M^+ activator were performed to provide further evidence of *Mt*IMPDH kinetic mechanism. In addition, we suggest that neither hydride transfer nor NADH release is the rate-limiting step. The chemical steps involved in the reactions catalyzed by IMPDH involve various proton transfers. Based on pH-rate profiles, amino acid residues involved in either catalysis or substrate binding are proposed.

Results and discussion

Amplification and cloning of *guaB2* gene

A PCR amplification product consistent with the expected *M. tuberculosis guaB2* (1590 bp) coding sequence was detected by agarose gel electrophoresis (data not shown), purified and inserted into the pCR-Blunt® vector. The cloned sequence was digested with *Nde*I and *BamH*I enzymes, purified and ligated into the pET-23a(+) expression

vector. Automated DNA sequencing confirmed the identity of the pET-23a(+)::*guaB2* construct and ensured that no mutations were introduced during PCR.

Expression and purification of the recombinant *Mt*IMPDH

The resulting pET-23a(+)::*guaB2* recombinant plasmid was transformed into C41(DE3) *E. coli* cells and cultures were grown in TB medium at 30 °C, for 36 h, as described in Experimental procedures section. Analysis by 12% sodium dodecyl sulfate-polyacrylamide gel eletrophoresis SDS–PAGE (data not shown) revealed expression in the soluble form of a protein with subunit molecular mass of approximately 55 kDa in agreement with the predicted MW for *Mt*IMPDH (54.7 kDa).

IMPDHs are readily purified using affinity chromatography[18,19,44] and ionic effects on protein stability and activity have been described,[45,46] as well as the ability of variou ions to induce the precipitation of proteins in solution. At high concentrations of salt, protein solubility drops sharply (salting-out) and this phenomenon forms the basis of many protein purification strategies.[47] Accordingly, recombinant *Mt*IMPDH protein was efficiently purified to homogeneity using a combination of $(NH_4)_2SO_4$ precipitation and a two-step protocol, consisting of an affinity column (HiTrap Blue HP) and a size exclusion column (HiLoad Superdex 200). Enzyme catalytic activity was measured in the standard assay (see Experimental procedures section), at saturating concentrations of IMP (1 mM) and NAD^+ (3 mM), for all purification steps. These enzyme activity measurements showed that indeed recombinant *Mt*IMPDH catalyzes the oxidation of IMP to XMP, with concomitant reduction of NAD^+ to NADH. The 1.7-fold purification protocol yielded 3 mg of recombinant protein from 3 g of cells, indicating 43% protein yield (Table 1). Total protein concentration was determined by the method of Bradford[48] and the homogenous *Mt*IMPDH was fast frozen in liquid nitrogen and stored at -80 °C.

Table 1

Purification protocol of recombinant *Mt*IMPDH from *E. coli* C41(DE3) (3 g wet cell paste)

Purification step	Total protein (mg)	Total enzyme activity (U)	Specific activity (U mg^{-1})	Purification fold	Yield (%)
Crude extract	11.6	13.9	1.2	1	100
HiTrap Blue HP	6.9	11.7	1.7	1.4	84
HiLoad Superdex 200	3.0	6.0	2.0	1.7	43

***Mt*IMPDH identification by Mass Spectrometry**

The identity of *Mt*IMPDH was confirmed by LC-MS/MS peptide mapping (see Experimental procedures section). Of 481 spectra, 52 different peptides were identified covering 96% of *Mt*IMPDH primary sequence.

Determination of *Mt*IMPDH molecular mass and structural characterization of K^+ binding

The average molecular mass of recombinant *Mt*IMPDH was determined using an Orbitrap analyzer (see Experimental procedures section). Peaks spanning charge states from 40+ to 71+ were detected. From the deconvoluted spectra, a value of 54,775 Da was found for the average molecular mass of recombinant *Mt*IMPDH. Interestingly, this experimentally determined molecular mass corresponds to the value expected for *Mt*IMPDH (with N-terminal methionine removed) with a single K^+ ion strongly associated with the enzyme (theoretical molecular mass of 54,774.9 Da). The MS analysis was repeated using homogeneous *Mt*IMPDH sample dialyzed against a buffer containing 200 mM NaCl instead of KCl salt. However, virtually the same result was obtained for the molecular mass of *Mt*IMPDH dialyzed against the NaCl-containing buffer (54,774 Da). These results showed that there exists a strong interaction between *Mt*IMPDH and K^+ that could not be weakened by extensive dialysis, probably corresponding to a structural K^+ ion bound to the enzyme.

In order to confirm the presence of K^+ ions and to determine the stoichiometry of protein subunits and ion species, homogeneous recombinant *Mt*IMPDH was analyzed

by Flame Atomic Absorption Spectroscopy (FAAS) and Inductively Coupled Plasma Optical Emission Spectroscopy (ICP-OES). A value of 1.08 (± 0.05) K^+ ions per *Mt*IMPDH subunit was determined, thereby lending support to formation a stable binary complex between *Mt*IMPDH and K^+, as suggested by the MS analysis.

Quaternary structure of *Mt*IMPDH

*Mt*IMPDH quaternary structure could not be assigned by analytical HPLC gel filtration chromatography because the enzyme eluted as different species depending on its concentration, indicating the presence of different aggregated forms. This elution profile was similar in the absence of an M^+, and in the presence of both K^+ (activator) and Na^+ (inhibitor), suggesting that M^+ activation (or inhibition) is not linked to protein oligomerization. Cross-linking experiments were thus performed and 12% SDS-PAGE analysis revealed the conversion from monomer to tetramer (*ca.* 220 kDa) after 10 min incubation time (Fig. 2). To ascertain whether the absence of M^+ and replacement of K^+ with Na^+ could affect the tetramer formation, *Mt*IMPDH was dialyzed against buffer A without M^+ and buffer A containing Na^+. No difference in the migration of polypeptide chains could be observed in 12% SDS-PAGE (data not shown). Molecular mass analysis of IMPDH from different sources, using a variety of methods, also provided evidence of higher-level association,[22,25,49-51] however the basis of this behavior has been only speculated.[22,49]At any rate, our results indicate that *Mt*IMPDH exists as tetramer and may form higher-order aggregates as observed for other IMPDHs.

Multiple sequence alignment

Crystal structures of IMPDHs from different organisms have been solved and allow drug design based on a detailed model of the target binding site. *M. tuberculosis* IMPDH shares 49%, 37%, 36%, 38% and 28% sequence identity with, respectively, *Pseudomonas aeruginosa* (PDB code: 3ZFH)[52], *Cryptosporidium parvum* (PDB code: 3FFS)[53], *Borrelia burgdorferi* (PDB code: 1EEP)[54], *Homo sapiens II* (PDB code: 1B3O)[55] and *Tritrichomonas foetus* (PDB code: 1AK5, 1ME8, 1LRT)[22,28,56] IMPDHs. These structures form homotetramers and are characterized by disorder that suggests a dynamic active site.[16]

Multiple sequence alignment was carried out and the results suggest that the key catalytic residue Cys331 (human type II numbering)[21] is conserved among the sequences (corresponding to Cys341 for *Mt*IMPDH), as are most of the residues that

interact with IMP (Fig. 3).[16,28] The conserved *Mt*IMPDH Ser339 and Tyr421 are equivalent to residues in *T. foetus* IMPDH that form hydrogen bonds to the ribose phosphate via their hydroxyl groups, while Gly376 and Gly397 (*M. tuberculosis* numbering) interact with the phosphate via main chain NHs. The amino acids Gly425, Ile340 and Glu458 (*M. tuberculosis* numbering) interact with the hypoxanthine ring of IMP in the *T. foetus* IMPDH.[28,57] These residues are conserved among the sequences aligned, except the Glu458 residue which is replaced with Gln441 in the human type II IMPDH (Fig. 3). The Asp374, which forms a hydrogen bond to the ribose moiety of XMP* is completely conserved among these IMPDHs (Fig. 3).[21] On the other hand, the amino acid Met424 (*M. tuberculosis* numbering) generally replaces the glutamate residue present in *T. foetus* IMPDH.[28]

The main differences among IMPDHs investigated to date are those associated with the flap and the NAD^+ binding site. The flap (residues 408-431 in the *T. foetus* IMPDH),[56] together with the active-site loop, form the active-site pocket. The flap is of great interest for species-selective inhibitor design as it is the least conserved region of the active site.[56] This flap displays varying degrees of flexibility and disorder depending upon the complexes formed.[16] The flap covers the IMPDH active site, and its distal portion moves in and out of the active site during the catalytic cycle, in which the open conformation is required for dehydrogenase reaction and closed conformation for hydrolysis of XMP* to yield XMP.[16] It is believed that the flap may be the key to understanding the coupling between the nicotinamide and adenosine sites.[28] The catalytic residues Arg443, which appears to act as a general base to activate water during the E-XMP* hydrolysis,[16] and Tyr444 in the mobile flap are conserved (Fig. 3).

Several inhibitors compete with the flap for the vacant NADH site, thus preventing the hydrolysis of E-XMP*.[16] The selectivity of these inhibitors is determined by both the structure of the NADH binding site and the dynamic properties of the flap. Microbial enzymes contain two different residues in the nicotinamide portion of the NADH site: Lys332 and Glu458 (*M. tuberculosis* numbering) are replaced with Arg and Gln (Fig. 3), respectively, in the human type II IMPDH. Site-direct mutagenesis studies of Lys and Glu residues of *T. foetus* IMPDH confirmed that these substitutions account for the species selectivity of MPA.[39] The crystal structure of the Chinese hamster IMPDH in complex with MPA and an IMP reaction intermediate (XMP*)[21] suggest that the conserved Thr343 (*M. tuberculosis* numbering) is likely to make direct contact with MPA. On the other hand, Ala285 replaces a serine residue which forms two hydrogen

bonds with the carboxylate group of the hexenoic acid moiety of MPA. Interestingly, the replacement of Ser276 (human type II numbering) with Ala disrupted this interaction and led to a 7-fold increase in apparent K_i.[21]

The amino acids Leu291 and Gly262 (*M. tuberculosis* numbering) replace, respectively, the Phe282 and His253 residues present in the human type II IMPDH, which stack with the adenine moiety of the dinucleotide.[55] These residues are not conserved among the IMPDHs (Fig. 3). The interactions between human type II IMPDH and the ribose of adenosine portion of the NAD analogue selenazole-4-carboxamide adenine dinucleotide (SAD) are between the Thr45 and Gln469 amino acids,[55] which are replaced with, respectively, Val60 and Gly486 in *Mt*IMPDH. Moreover, a leucine residue in the *P. aeruginosa*, *C. parvum* and *B. burgdorferi* IMPDHs substitutes for Thr45 in human type II IMPDH. Altogether, these amino acid sequence comparisons suggest that it may be possible to exploit the differences among microbial and mammalian IMPDHs to develop selective inhibitors.

Apparent steady-state kinetics

The apparent steady-state parameters were collected under standard assay conditions (see Experimental procedures section). The dependence of velocity on increasing concentrations of NAD^+ (Fig. 4A), at saturating IMP concentration (1 mM), revealed substrate inhibition at high NAD^+ levels (> 3 mM), as had been reported by Chen *et al*.[38] The apparent steady-state parameters derived from data fitting to Eq. (1) yielded the following values: k_{cat} = 3.10 (± 0.04) s^{-1}, K_m^{NAD} = 887 (± 36) μM. More appropriately, data fitting to Eq. (2) to account for substrate inhibition yielded values of 5.2 (± 0.8) s^{-1} for k_{cat}, 1.9 (± 0.5) mM for K_m^{NAD}, and 6.3 (± 1.9) mM for K_i. The latter results are in reasonably good agreement with values reported by Chen *et al*.[38] for K_m^{NAD} (1 mM) and K_i (5 mM), except for k_{cat} (0.53 s^{-1}). This discrepancy in k_{cat} values is likely due the lower temperature of assay measurements used by Chen *et al*. (25 ºC) as compared to 37 ºC for the results here described. The K_m^{NAD} value is larger than that reported by Usha *et al*.[41] (610 μM), which was derived from data fitting to Michaelis-Menten equation in the absence of substrate inhibition (varying NAD^+ concentration from 0.03 to 4.5 mM). The substrate inhibition is commonly observed in IMPDHs and has been reported to be uncompetitive,[9,18,25,58] presumably resulting from the formation of a nonproductive E-XMP*-NAD^+ complex.[20] This behavior also suggests that product

dissociation follows an ordered mechanism, in which NADH is the first product released.[59]

No *Mt*IMPDH catalytic activity could be detected for varying nicotinamide adenine dinucleotide phosphate ($NADP^+$) concentrations up to 20 mM. The NAD^+ analog acetylpyridine adenine dinucleotide ($APAD^+$) is a substrate for *Mt*IMPDH and the dependence of velocity on increasing concentrations of $APAD^+$ (Fig. 4B) also displayed substrate inhibition. The apparent steady-state parameters derived from data fitting to Eq. (2), which accounts for substrate inhibition, yielded values of 5.4 (± 0.6) s^{-1} for k_{cat}, 2.0 (± 0.4) mM for K_m^{APAD}, and 5 (± 1) mM for K_i. The calculated values for the apparent specificity constants (k_{cat}/K_m) for NAD^+ and $APAD^+$ are, respectively, 2.7 (± 0.7) x 10^3 $M^{-1}s^{-1}$ and 2.7 (± 0.5) x 10^3 $M^{-1}s^{-1}$, employing the apparent steady-state kinetic parameters derived from data fitting to Eq. (2). Despite the differences in the structures and reduction potentials between NAD^+ and $APAD^+$,[60] the k_{cat} values are comparable. This observation suggests that hydride-transfer is likely not rate-limiting since this rate should be different for reduced APADH.[16] Moreover, uncompetitive substrate inhibition versus IMP represents additional evidence that the release of XMP can limit the overall reaction.[59] NADH release and E:XMP* hydrolysis have been proposed to be rate-limiting steps for *T. foetus* IMPDH catalysis.[20] On the other hand, hydrolysis of a covalent enzyme intermediate has been proposed to be rate-limiting for *C. parvum* IMPDH reaction.[20,30,58]

The saturation curve for IMP (Fig. 5A) deviates from Michaelis-Menten kinetics, and it appears to exhibit cooperative kinetics. Experimental data were thus fitted to the Hill equation, Eq. (3), with values of k_{cat} = 2.20 (± 0.02) s^{-1}, $K_{0.5}$ = 120 (± 2) μM and n = 1.51 (± 0.04). The Hill coefficient (n) value larger than one suggests positive cooperativity,[61] although moderate. To ascertain whether or not *Mt*IMPDH dependence on IMP concentration was best described by a sigmoidal rather than a hyperbolic (Eq. 1) system, the residuals (*i.e.*, the differences between the predicted and observed values of the dependent variables) of data fitting to, respectively, Eq. (3) (Fig. 5A) and Eq. (1) (Fig. 5B) were analyzed. This straightforward analysis lends support to the proposal that IMP kinetics is best described by a cooperative system (Fig. 5A - inset) as compared to a Michaelis-Menten one (Fig. 5B - inset), as the latter shows a systematic deviation from the theoretical values. In this case (n > 1), the binding of one IMP molecule increases the affinity of a second molecule of substrate to the protein active site.

To the best of our knowledge, this is the first example of an IMPDH enzyme that shows sigmoidal dependence of velocity on ligand concentration. Nevertheless, titration calorimetry of ligand binding revealed that IMP can interact with hamster IMPDH type II in a negatively cooperative manner and showed evidence this enzyme is an allosteric protein.[62] Moreover, previous work reported that GMP induces cooperativity between IMP binding sites for *E. coli* IMPDH.[63] Interestingly, the k_{cat} and $K_{0.5}$ values for IMP, at saturating concentration of $APAD^+$ (3 mM), were similar to those measured at saturating concentration of NAD^+ (data not shown).

The k_{cat} values are similar to those reported for bacterial[18,25] and parasitic IMPDHs,[20,58] and the K_m and K_i values for NAD^+ are in reasonably good agreement with those previously reported for *Mt*IMPDH.[38,41] On the other hand, the k_{cat} value for *Mt*IMPDH is larger than that for human type II IMPDH,[29] implying that the rate of hydrolysis of E-XMP* can be greater and that the *Mt*IMPDH resistance to MPA[38] would result from this feature.[36,64]

Monovalent cation (M^+) activation

The activation of IMPDHs by M^+ is well documented, although the cation specificity varies for IMPDHs from different sources.[16] Usha *et al.*[41] have recently reported that K^+ promotes the maximal catalytic activity for *Mt*IMPDH. To further characterize the effect of M^+ on *Mt*IMPDH activity, the dependence of reaction velocity on increasing concentrations of K^+, NH_4^+, Rb^+ and Cs^+ was evaluated. The saturation curves displayed hyperbolic kinetics (data not shown) and the steady-state kinetics parameters were thus obtained from data fitting to Eq. (1). These parameters are given in Table 2. The results indicate that K^+, NH_4^+ and Rb^+ are the most effective activators, while Cs^+ produces the lowest increase in activity. Despite a slight variation on the k_{cat} values, the k_{cat}/K_m for K^+ and NH_4^+ are equivalent and fairly close to Rb^+ (Table 2), as observed for other IMPDHs.[16] The activation by, and similar steady-state parameters for, K^+, NH_4^+, and Rb^+ are not surprising as these cations have similar values for ionic radii in crystals, ion mobility, and estimated size of hydrated ion.[66]

Table 2

Apparent kinetic constants for monovalent cations[a].

Cation	Ionic radius[b] (Å)	k_{cat} (s^{-1})	K_m (mM)	k_{cat}/K_m ($M^{-1}s^{-1}$)	K_{is} (mM)[c]	K_{ii} (mM)[d]
Li^+	0.60	n.a.[e]	n.a.[e]	n.a.[e]	129 ± 16	380 ± 52
Na^+	0.95	n.a.[e]	n.a.[e]	n.a.[e]	108 ± 16	708 ± 176
K^+	1.33	2.83 ± 0.09	37 ± 5	76 ± 10	n.a.[e]	n.a.[e]
NH_4^+	1.48	2.08 ± 0.04	28 ± 2	74 ± 5	n.a.[e]	n.a.[e]
Rb^+	1.48	2.08 ± 0.09	44 ± 6	47 ± 6	n.a.[e]	n.a.[e]
Cs^+	1.69	0.76 ± 0.05	84 ± 13	9 ± 1	n.a.[e]	n.a.[e]

[a] All assays were performed as described in the Experimental procedures section.

[b] The values for cation radii from crystal data were taken from references[65,66].

[c] K_{is} = the slope inhibition constant.

[d] K_{ii} = the intercept inhibition constant.

[e] Not applicable.

It is noteworthy that neither Na^+ nor Li^+, which have lower ionic radii than K^+, activated the *Mt*IMPDH. On the contrary, they inhibit the K^+-activated *Mt*IMPDH, acting as noncompetitive inhibitors (Table 2). Divalent cations, such as Mg^{2+} and Ca^{2+}, also did not activate this enzyme even at 200 mM. These results suggest the requirement of M^+ for increased enzyme activity, and that ionic radius plays a role in monovalent cation specificity as the k_{cat}/K_m for Cs^+ is smaller than those for K^+, NH_4^+, and Rb^+ (Table 2).

Enzymes activated by metals evolved to take advantage of the large availability of Na^+ outside the cell and K^+ inside the cell to optimize their catalytic function. Indeed, a strong correlation exists between the preference for K^+ or Na^+ and the intracellular or extracellular localization of such enzymes.[67] *M. tuberculosis* has evolved multiple mechanisms to survive within the host alveolar macrophages[68,69] and has adapted its lifestyle to accommodate the changing environment within the phagosomes.[70] The abundance of K^+ in physiological environments[71] and the analysis of K^+ concentration inside phagosomes of macrophages infected with mycobacteria,[70] would probably explain the *Mt*IMPDH preference for this cation.

To further characterize the selectivity for M^+, the effects of K^+, NH_4^+ and Rb^+ on the apparent kinetic parameters for IMP and NAD^+ were studied. These experiments could not be carried out in the presence of Cs^+ as a consequence of the reduced rate

obtained with this cation that precluded acquisition of reliable data. The $K_{0.5}$ and K_m values for the substrates were nearly identical, resulting in minor differences in their k_{cat} values (data not shown), suggesting that M^+ does not interact directly with the substrates or that it is not related with substrate binding affinity, as previously observed.[19,72,73] Notwithstanding, site-direct mutagenesis and crystallographic studies will have to be pursued to assign any relationship between substrate binding and M^+ activation for *Mt*IMPDH.

The mechanism of K^+ activation is not completely understood, although it does not appear to affect the formation of IMPDH tetramers.[18,19] The crystal structures of IMPDHs from Chinese hamster[21]and *T. foetus*[56,57] have revealed the presence of a potassium-binding site near the active cysteine, which is located in a glycine-rich loop. The carbonyl oxygen from the catalytic Cys319 (*T. foetus* numbering) forms part of the cation-binding site and when this site is occupied, the cysteine is in a favorable position to form the covalent bond with the C2 carbon of IMP.[56] This observation suggests that this ion is important in coordinating the active cysteine residue in an orientation required for catalysis. In this case, stabilization of the Cys319 loop provides an explanation for K^+ activation.

It has been shown that K^+ does not affect the rate of 6-chloro-purine ribotide (6-Cl-PRT) inactivation of human type II IMPDH, nor the hydrolysis of 2-chloro-IMP by this enzyme.[72] This finding is in agreement with previous equilibrium binding studies which showed the presence of one binding site per subunit for IMP and XMP even in the absence of K^+,[19] demonstrating that the M^+ activator does not modulate the reactivity of the sulfhydryl group. Kinetic and mutagenesis studies have argued for a link between potassium ion and conformational changes involved in NAD^+ binding.[26,72,74,75] More recently, based on kinetic and free energy simulations analyses, Riera *et al*. showed that K^+ accelerates IMPDH conformational transitions that facilitate the dinucleotide binding steps in *C. parvum* IMPDH.[73] Riera *et al*. have also demonstrated that the K^+ dependence of k_{cat} derives from the rate of flap closure, which increases in the presence of this cation.[73] The model put forward by Riera *et al*. suggests that K^+ preorganizes IMPDH protein thereby decreasing the activation barrier for flap closure.[73] In addition, these authors presented computational simulation results showing that K^+ mobilizes residues on the Cys319 loop by providing alternative interactions for the main chain carbonyl oxygens, facilitating the conformational changes required for completion of the catalytic cycle.[73] Incidentally, Riera *et al*. have chosen *C. parvum*

IMPDH enzyme to carry out these studies as it contains only one conserved monovalent cation binding site.[73]

Here, we have shown by Mass Spectrometry, FAAS and ICP-OES spectroscopy analysis that the apo form of *Mt*IMPDH stably binds K^+ ions in a 1:1 stoichiometry. This ion-protein interaction detected is strong enough to withstand the harsh conditions of electrospray ionization, suggesting that it is likely a structural ion. On the other hand, the activation mediated by K^+ detected in *Mt*IMPDH kinetic analysis may suggest a second K^+ binding site, probably representing the K^+ binding site previously reported in the hamster E-XMP*-MPA complex, which may be catalysis-dependent.[21] However, ideally, crystal structure of *Mt*IMPDH with K^+ ion(s) bound should be provided to both ascertain whether or not there are two metal binding sites and its/their mechanism of activation. Interestingly, it has recently been pointed out that those crystal structures of IMPDHs that do not include K^+ are unlikely to be catalytically relevant.[31]

Initial velocity patterns

A complete mechanism for *Mt*IMPDH catalysis should take into account the monovalent cation as it has been shown here that addition of K^+ is required for increased enzyme activity. To determine the true steady-state kinetic parameters and to provide information about the *Mt*IMPDH enzyme mechanism in the presence of K^+, initial velocity as a function of substrate concentration (NAD^+ or K^+) was plotted as a linear function of double reciprocal of initial velocity against the reciprocal of substrate concentration. It should be pointed out, however, that plots for increasing IMP concentrations were not included in the analysis since kinetic data deviated from linearity (n = 1.51) at low concentrations and saturating levels of NAD^+ and K^+. Intersecting families of double-reciprocal (Lineweaver-Burk) plots were obtained for both NAD^+ (Fig. 6A and 6C) and K^+ (Fig. 6B and 6D). These patterns are consistent with a sequential mechanism.[76] Data were plotted in reciprocal form and fitted to the equation for a sequential initial velocity pattern (Eq. (4)), and the true steady-state parameters are summarized in Table 3. Interestingly, a sequential mechanism has also been reported for the bacteria *Aerobacter aerogenes*,[74] human type II[29] and the protozoan parasite *T. foetus* IMPDHs.[20,77]

Table 3

Kinetic parameters obtained from initial velocity studies of *Mt*IMPDH[a].

Varied substrate / cofactor[b]	Fixed substrate[c]	k_{cat} (s^{-1})	K_m^{NAD} (μM)	K_m^{K} (mM)
NAD^+ against K^+	IMP	3.7 ± 0.1	1092 ± 74	102 ± 6
NAD^+ against IMP	K^+	3.1 ± 0.1	794 ± 57	n.a.[d]
K^+ against IMP	NAD^+	3.3 ± 0.1	n.a.[d]	44 ± 3

[a] All assays were performed as detailed in the Experimental procedures section.

[b] In all of the pairs of varied substrates, the first one was varied and the second was maintained at different fixed-varied concentrations.

[c] All of the fixed substrates were maintained at saturating concentrations.

[d] Not applicable.

Inhibition studies

The initial velocity studies described above ruled out ping-pong and rapid equilibrium ordered mechanisms as the former gives double reciprocal plots displaying parallel lines and the latter a family of lines intersecting on the *y*-axis.[76] However, these data cannot distinguish between a steady-state ordered mechanism and rapid equilibrium random system.[76] Accordingly, product (either XMP or NADH) inhibition measurements were carried out to elucidate the order, if any, of substrate addition to *Mt*IMPDH enzyme. Remarkably, when NAD^+ and K^+ were fixed at non-saturating concentrations ($\cong K_m$), IMP double-reciprocal plots were linear. Accordingly, inhibition studies could also be carried out as a function of IMP concentrations. Product inhibition data were fitted to equations for competitive (Eq. (5)) and noncompetitive (Eq. (6)) inhibition. Table 4 summarizes the product inhibition patterns and the respective inhibition constants. The results showed a pattern of competitive inhibition of XMP with respect to IMP (Table 4). The remaining three inhibition patterns were noncompetitive (Table 4). These results are consistent with a steady-state ordered Bi Bi kinetic mechanism, in which IMP binds to free *Mt*IMPDH enzyme first followed by NAD^+ binding to form the catalytically competent ternary complex. The substrate inhibition, which is more common in steady-state ordered mechanisms, when one substrate resembles one of the products structurally,[59] is in agreement with our observations. Moreover, the noncompetitive inhibition profile of NADH requires that E·XMP (or E-XMP*) exist in the steady-state, so that release of XMP may be at least one of the slow steps along the reaction pathway.

However, these results are different from the random mechanism reported for the *T. foetus*[20] and human type II IMPDHs[29,30] based on measurements of isotope effects and transient kinetics. It should be pointed out that the ordered addition of substrates to IMPDH enzymes has been called into question.[16] However, the order of product release appears to hold for IMPDHs.[16]

The product inhibition results showed that XMP and NADH are noncompetitive inhibitors with respect to K^+ (Table 4). These data suggest that XMP and NADH products can bind to *Mt*IMPDH regardless the presence or absence of added K^+. As described above, FAAS, ICP-OES and MS data suggest formation of a stable binary complex between *Mt*IMPDH and K^+.

Table 4

Product inhibition patterns for *Mt*IMPDH[a].

Variable substrate	Inhibitor	Type of inhibition	K_{is} (μM) [b]	K_{ii} (μM) [c]
IMP	XMP	competitive	0.26 (± 0.03) x 10^{+3}	n.a.[d]
IMP	NADH	noncompetitive	0.4 (± 0.1) x 10^{+3}	0.47 (± 0.07) x 10^{+3}
NAD^+	XMP	noncompetitive	1.9 (± 0.4) x 10^{+3}	1.3 (± 0.1) x 10^{+3}
NAD^+	NADH	noncompetitive	0.31 (± 0.06) x 10^{+3}	0.9 (± 0.2) x 10^{+3}
K^+	XMP	noncompetitive	0.46 (± 0.05) x 10^{+3}	2.6 (± 4) x 10^{+3}
K^+	NADH	noncompetitive	0.36 (± 0.09) x 10^{+3}	0.41 (± 0.05) x 10^{+3}

[a] All assays were performed as described in the Experimental procedures section.

[b] K_{is} = the slope inhibition constant.

[c] K_{ii} = the intercept inhibition constant.

[d] Not applicable.

It has been shown that GMP, the product of the next reaction in the *de novo* guanine nucleotide pathway, is a common inhibitor for IMPDHs.[18,44,74,78] To evaluate the inhibitory effect of GMP on *Mt*IMPDH enzyme velocity, measurements of steady-state rates were carried out as described in the Experimental procedures section. The double-reciprocal plots at different GMP concentrations as a function of either IMP (Fig. 7A) or NAD^+ (Fig. 7B) displayed distinct patterns. GMP usually acts as a competitive inhibitor towards IMP.[18,49,74] However, this appears not to hold for *Mt*IMPDH as GMP showed a pattern of noncompetitive inhibition with respect to IMP. Data fitting to Eq. (6) yielded K_{is} and K_{ii} values of, respectively, 0.47 (± 0.05) x 10^{+3} μM and 4.0 (± 0.6) x 10^{+3} μM. The inhibition pattern of parallel lines indicates that

GMP acted as an uncompetitive inhibitor with respect to NAD^+, in which both V_{max} and K_m values were simultaneously reduced. Data fitting to Eq. (7) for uncompetitive inhibition yielded a K_{ii} value of 0.40 (± 0.03) x 10^{+3} μM. These results suggest that GMP may act as a negative feedback regulator of the mycobacterial enzyme, maintaining a balance of the guanine nucleotides synthesis in the cell. On the other hand, GTP did not inhibit *Mt*IMPDH as has been reported for *Leishmania donovani* IMPDH.[44]

In an attempt to find nucleotides that can act as regulators of *Mt*IMPDH, the dependence, if any, of enzyme velocity on increasing IMP and NAD^+ concentrations was evaluated. These measurements were carried out in the presence of a fixed concentration (500 μM) of AMP, ATP, UTP and CTP, and compared to *Mt*IMPDH rates in the absence of these nucleotides. No noticeable effect on the *Mt*IMPDH kinetic properties towards IMP and NAD^+ could be observed. These results are in agreement with data showing that IMPDHs are not allosterically regulated by these nucleotides.[16]

pH-rate profiles

The dependence of kinetic parameters on varying pH values was carried out to probe acid-base catalysis and to gain information on the chemical mechanism of *Mt*IMPDH. The pH-rate profiles obtained for the *Mt*IMPDH reaction show catalysis decrease in the acidic limb with a slope of +1, indicating that protonation of a single group abolishes activity (Fig. 8A).[79] Data fitted to Eq. (8) indicate that deprotonation of a group with p*K* value of 8.2 (± 0.6) plays a critical role in *Mt*IMPDH catalysis. IMP and NAD^+ have no dissociating groups with this p*K* value, indicating that this group is probably an amino acid chain of the enzyme.[72] This p*K* value has been shown to reflect the ionization of the reactive Cys331 (human type II numbering) thiol group in the free enzyme which must be deprotonated to attack the C2 of IMP in the course of catalysis.

The cysteine thiol group usually ionizes at slightly alkaline pH values, and the resulting thiolate anion is the reactive species that acts as a nucleophile, which is one of the most reactive functional groups found in proteins.[80] In addition, the ability of the thiol residue to ionize appears to be critical for the reaction involving nucleophilic attack, since the Cys331Ala mutation abolished IMPDH activity.[21,75] The active site Cys331 has been clearly identified by the use of irreversible inhibitors,[81] isolation of enzyme intermediates under turnover conditions as well as direct observation by X-ray crystallography.[21,32] Sintchak *et al*.[21] solved the crystal structure of the Chinese hamster

IMPDH in complex with MPA and an IMP reaction intermediate (XMP*) that is generated during substrate turnover, and demonstrated that both molecules are simultaneously bound in the active site. This IMPDH structure also revealed a covalent adduct between Cys331 and the C2-position of the XMP*, confirming cysteine role in catalysis. In the *T. foetus* IMPDH crystal structure, this residue is located in a disordered loop, suggesting a high degree of flexibility needed for the catalytic cycle to occur,[22] but which becomes ordered during ternary complex formation.[28] Based on these observations, it is thus tempting to suggest that the cysteine (Cys341 in *Mt*IMPDH) side chain is the general basic group whose protonation abolishes the *Mt*IMPDH catalytic activity.

The bell-shaped pH-rate data for k_{cat}/K_{NAD+} (Fig. 8B) were fitted to Eq. (9), yielding apparent p*K* values of 7.5 (± 0.7) and 9.0 (± 0.6), for groups that must be deprotonated and protonated, respectively, for NAD^+ binding. Slopes of +1 for the acidic limb and -1 for the basic limb indicate participation of a single ionizable group in each limb. It has been pointed out that the p*K* value obtained for the acidic group may reflect the ionization of the reactive cysteine thiol group in altered environments.[82] A group with a p*K* value of 6.9 (± 0.2) was also found to be important for substrate binding to human type II IMPDH and, since NAD^+ does not have p*K* values in this range, the authors have suggested that the ionizing groups are located in the enzyme·IMP complex. The rate of inactivation of the enzyme by 6-Cl-PRT as a function of pH was also determined, assigning the thiol group of Cys331 as the residue with a p*K* value of 7.5 (± 1).[72] Accordingly, it is likely that the p*K* values in the acidic limb for both k_{cat} and k_{cat}/K_{NAD+} are reporting on the same group.

The crystal structure of *T. foetus* IMPDH showed that the carboxamide group of the NAD^+ analogue *β*-methylene-TAD forms hydrogen bonds with Ser262, Gly312, Gly314, and Arg322.[28] The amino acid side chain having a pK_a value of 9.0 that has to be protonated for NAD^+ binding to *Mt*IMPDH (Fig. 8B) may thus tentatively be ascribed to the Arg344 (*M. tuberculosis* numbering) residue conserved in bacterial IMPDHs (Fig. 3).

The pK_a value of the δ-guanido group of arginine in solution is usually about 12. How can one reconcile the pK_a value of 9.0 for amino acid side chains involved in NAD^+ binding? It has been pointed out by Copeland[83] that in some cases the pK_a values that are measured cannot be correctly ascribed to a particular amino acid, but rather reflect a specific set of residue interactions within an enzyme molecule that create *in*

situ a unique acid-base center. Moreover, the hydrophobic interior of enzyme active sites that undergo domain closure can greatly perturb the pK_a values of amino acid side chains relative to their typical pK_a values in aqueous solution. Notwithstanding, site-direct mutagenesis and crystal structure determination will have to be pursued to assign any role in substrate binding and catalysis to a particular amino acid residue in *Mt*IMPDH.

The pH dependence on IMP binding was not included in the analysis, since saturation curves were sigmoidal. However, measurements of initial velocities as a function of increasing IMP concentrations over pH values ranging from 7.0 to 10.0 showed that the cooperative index (n) of IMP increases with decreasing pH values (Table 5). It is interesting to note that, as has been pointed out in a review showing a timeline of evolution of allostery as a concept,[84] pH is now considered an allosteric effector. In addition, it could be observed that at higher pH levels, both k_{cat} and $K_{0.5}$ values were simultaneously increased. The increase in k_{cat} value as a function of increasing pH value is not surprising as protons are released in solution in the course of IMPDH-catalyzed chemical reaction. On the other hand, the $K_{0.5}$ dependence on pH values may represent an additional evidence of *Mt*IMPDH cooperativity for IMP substrate.

Table 5

pH dependence of the IMP kinetic parameters[a].

pH	k_{cat} (s^{-1})	n[b]	$K_{0.5}$ (μM)[c]
7.0	0.202 ± 0.003	2.4 ± 0.2	93 ± 3
7.5	0.755 ± 0.005	1.84 ± 0.06	58 ± 1
8.0	1.39 ± 0.02	1.7 ± 0.1	69 ± 2
8.5	2.24 ± 0.01	1.58 ± 0.04	106 ± 1
9.0	2.55 ± 0.05	1.5 ± 0.1	148 ± 6
9.5	3.4 ± 0.2	1.1 ± 0.1	348 ± 36
10.0	3.06 ± 0.08	1.18 ± 0.05	1077 ± 62

[a] All assays were performed as described in the Experimental procedures section.

[b] n = the Hill coefficient

[c] $K_{0.5}$ = a constant correlated to K_m which contains terms related to the effect of substrate occupancy at one site on the substrate affinity of other sites.

Energy of activation

The energy of activation for the enzyme-catalyzed chemical reaction was assessed by measuring the dependence of k_{cat} (s^{-1}) on temperature (Fig. 9). These data were calculated by determining the slope of the Arrhenius plot (Eq. (10)), yielding a value of 7.5 kcal mol^{-1}, which represents the minimal amount of energy required to initiate the *Mt*IMPDH-catalyzed chemical reaction,[85] since we measured the enzyme activity at saturating concentrations of substrates. The linearity of the Arrhenius plot also suggests that there is no change in the rate-limiting step over the temperature range utilized in the assay.

Conclusion

The identification of new metabolic targets has been a challenge in the search for anti-mycobacterial agents. Inosine 5'-monophosphate dehydrogenase (IMPDH) is the rate-limiting enzyme in the *de novo* biosynthesis of guanine nucleotides. Bacterial and mammalian IMPDH enzymes appear to have unique structural and biochemical characteristics, which have been exploited in the development of species-selective inhibitors.[32,34,35] *Mt*IMPDH appears to be a promising drug target as DNA metabolism is maintained in both active and latent forms of TB, and the purine biosynthesis has been predicted to be essential for mycobacteria *in vitro* growth.[42] The results here described showed that *Mt*IMPDH displays kinetic properties typical of bacterial IMPDHs, although with particular characteristics. For instance, the sigmoidal dependence of enzyme velocity on increasing IMP concentrations suggests cooperative kinetics, and the noncompetitive inhibition pattern for GMP with respect to IMP suggests allosteric regulation. It has been pointed out that IMPDH reaction involves several conformational rearrangements [20,28,31] and that M^+ activation may be an example of allostery for some IMPDHs.[67,73] In any case, allostery appears to be an intrinsic IMPDH property during the catalytic cycle. Such allosteric signals can arise from a variety of mechanisms, and growing evidence supports the notion that many, if not all, proteins utilize allostery.[86] Regulation of activity through metal ion complexation plays a key role in many enzyme-catalyzed reactions and over one-third of known proteins are metalloproteins.[67] A kinetic analysis of metal interactions and *Mt*IMPDH has been described. The requirement of M^+ for the *Mt*IMPDH activity has been demonstrated and the Michaelis constants for these ions determined. Nevertheless, *Mt*IMPDH structural

information of M^+ binding sites has to be pursued to provide the molecular basis for cation activation. In addition, here a sequential kinetic mechanism is proposed for *Mt*IMPDH based on steady-state kinetics, which is consistent with ternary complex formation, as well as an ordered addition of substrates and release of products, supported by product inhibition studies, with K^+ association as the catalysis proceeds.

The potential of IMPDH in antimicrobial chemotherapy is beginning to be exploited as recent reports of parasite-selective inhibitors.[34,35] The target-based rational design of new agents with anti-TB activity includes functional and structural efforts. Accordingly, mechanistic analysis should be included in enzyme-targeted drug programs aiming at the rational design of potent enzyme inhibitors. Understanding the mode of action of *Mt*IMPDH will inform us on how to better design inhibitors targeting this enzyme. Moreover, elucidation of particular signatures of the *Mt*IMPDH will provide insight into the catalytic mechanism of this enzyme and the foundation for the development of specific inhibitors.[46] These inhibitors may also be useful tools to chemical biologists for loss-of-function experiments to reveal the biological role of *Mt*IMPDH in the context of whole *M. tuberculosis* cells. In addition, it is hoped that the results here described may contribute to our understanding of the biology of *M. tuberculosis*.

Experimental procedures

Materials

Oligonucleotide primers were synthesized by Invitrogen. All restrictions enzymes were purchased from New England Biolabs and thermostable *Pfu*® DNA polymerase was from Stratagene. Quick Gel Extraction kit, T4 DNA ligase and pCR-Blunt® vector were from Invitrogen and Qiaprep Spin Miniprep kit was from Qiagen. *E. coli* strains and pET-23a(+) expression vector were purchased from Novagen. Chemicals were of analytical or reagent grade and were obtained from Sigma-Aldrich, except for XMP and dithiothreitol (DTT) that were from, respectively, Santa Cruz Biotechnology and Acros Organics. All purification steps were carried out on an ÄKTA system (GE Healthcare) at 4 ºC with UV detection at 215, 254 and 280 nm, and fractions were analyzed by 12% SDS-PAGE stained with Coomassie Brilliant Blue.[87] AMICON stirred ultrafiltration cell, regenerated cellulose ultrafiltration membranes were from Millipore Corporation. Bovine serum albumin and Bradford reagent were from Bio-Rad Laboratories. Linbro

cell culture plate was from MP Biomedical, Inc. Siliconized coverslips and vacuum grease sealant were purchased from Hampton Research. The mass spectrometer LTQ-XL and LTQ Orbitrap Discovery were from Thermo and the nanoLC Ultra 1D plus was from Eksigent. Steady-state kinetic experiments were performed on an UV-2550 UV/Visible spectrophotometer (Shimadzu).

Amplification, cloning and DNA sequencing of the *guaB2* gene

Primers were designed using the annotated *M. tuberculosis guaB2* gene (Rv3411c) sequence available on Tuberculist database.[88] Synthetic oligonucleotides used (forward primer, 5′-CACATATGTCCCGTGGCATGTCCGGCCTG-3′; and reverse primer, 5′-GGGGATCCTCAGCGCGCGTAGTAGTTGG-3′) were designed to contain, respectively, *Nde*I and *BamH*I restriction sites (underlined). The full-length *guaB2* coding region (1590 bp) was PCR amplified using the genomic DNA from *M. tuberculosis* H37Rv as template and a high fidelity proof-reading thermostable *Pfu*® DNA polymerase, in the presence of 10% dimethyl sulfoxide (DMSO, final concentration). The isolated DNA fragment was cloned into pCR-Blunt® vector, transformed into *E. coli* strain DH10B and selected on LB medium containing 50 μg mL^{-1} kanamycin. The resulting plasmid was isolated utilizing the Qiaprep Spin Miniprep kit. Subsequently, the fragment was cleaved with *Nde*I and *BamH*I endonucleases and inserted into the pET-23a(+) expression vector, previously treated with the same restriction enzymes. The complete *guaB2* nucleotide sequence was determined by automated DNA sequencing to corroborate sequence identity, integrity and to check the absence of mutations in the cloned fragment.

Expression of recombinant *Mt*IMPDH

The recombinant plasmid pET-23a(+)::*guaB2* was transformed into C41(DE3) *E. coli* electrocompetent host cells, and cells carrying the recombinant vector were selected on LB agar plates containing 50 μg mL^{-1} ampicillin.[89] A single colony was used to inoculate 50 mL of LB medium containing the same antibiotic and grown overnight at 37 ºC. Aliquots of this culture (5 mL) were used to inoculate 500 mL of Terrific Broth (TB) medium in 5 x 1 L flasks supplemented with ampicillin (50 μg mL^{-1}) and grown at 37 ºC and 180 rpm to an optical density (OD_{600nm}) of 0.4 – 0.6. At this growth stage, the temperature was lowered to 30 ºC and 0.5 mM of isopropyl-β-D-thiogalactopyranoside (IPTG) was added to induce protein expression. After 36 h, the cells (19 g) were

harvested by centrifugation, at 11,800*g* for 30 min at 4 °C and stored at -20 ºC. The same protocol was employed for C41(DE3) *E. coli* cell transformed with pET-23a(+) as control. The expression of the recombinant protein was confirmed by 12% SDS-PAGE and Coomassie Brilliant Blue staining.

Purification of recombinant *Mt*IMPDH

All subsequent steps were carried out at 4 ºC, unless otherwise specified. Approximately 3 g of wet cell paste were suspended in 30 mL of 50 mM tris(hydroxymethyl)aminomethane (Tris, buffer A) pH 7.5. Cells were disrupted by sonication (ten pulses of 10 s, with cooling intervals of 1 min, at 60% amplitude) and the lysate was centrifuged at 38,900*g* for 30 min to remove cell debris. The supernatant was treated with buffer A containing 2 M $(NH_4)_2SO_4$, to a final concentration of 1 M, stirred for 30 min, and centrifuged at 38,900*g* for 30 min. The resulting precipitate containing *Mt*IMPDH was resuspended in 8 mL of buffer A (crude extract) and loaded on a 5 mL HiTrap Blue HP column, pre-equilibrated with buffer A. The column was washed with 15 column volumes of buffer A, and the protein elution was carried out using a 0-900 mM NaCl linear gradient in buffer A (25 column volumes), at a flow rate of 1 mL min^{-1}.

Fractions containing *Mt*IMPDH in NaCl (*ca.* 600 mM) were pooled and concentrated to approximately 8 mL using an AMICON ultrafiltration membrane (MWCO = 10 kDa). The soluble sample was loaded on a HiLoad Superdex 200 26/60 size exclusion column, which was previously equilibrated with buffer A. Proteins were isocratically eluted at 1 mL min^{-1} flow rate, and fractions containing the homogeneous *Mt*IMPDH were pooled, concentrated and stored at -80 °C. Protein concentration was determined by Bradford's method,[48] using serum albumin as standard.

***Mt*IMPDH identification by mass spectrometry**

Aliquots of 1 nmol of *Mt*IMPDH were digested with trypsin and the peptides were separated by nanochromatography (nanoLC Ultra 1D plus – Eksigent, USA) using 15 cm capillary columns (150 µM i.d., Kinetex C18 core-shell particles – Phenomenex, Inc.). The separated peptides were detected by mass spectrometry using an LTQ-Orbitrap hybrid mass spectrometer (Thermo Electron Corporation). The chromatographic method used a linear gradient from mobile phase A (0.1% formic acid in water) to mobile phase B (0.1% formic acid in acetonitrile) of 2-80% B over 60 min.

We performed MS/MS fragmentation using collision-induced dissociation (CID) with an activation Q of 0.250, an activation time of 30.0 ms, and an isolation width of 1.0 Da. Using the Proteome Discoverer software (v. 1.3), we compared experimentally obtained MS and MS2 spectra with the *in-silico* trypsin digestion of the *M. tuberculosis* H37Rv proteome. We allowed a precursor tolerance of 10 ppm, a fragment tolerance of 0.8 Da, static carbamidomethylation on cysteines, and oxidation on methionine residues. We restricted our analysis to matches with a Xcorr score > 2.0 for doubly charged ions and Xcorr score > 2.5 for triply charged ions.

Determination of *Mt*IMPDH molecular mass

Homogeneous samples of *Mt*IMPDH were desalted, reconstituted in acetonitrile 50%:water 47%:formic acid 3% and directly injected into an IonMax electrospray ion source. The electrospray parameters were as follows: positive ion mode, 4 kV of applied voltage, 25V of capillary voltage, 300 °C of capillary temperature, and 94 V of tube lens voltage. High-resolution full spectra (750-2000 m/z range) were collected on a Thermo Orbitrap Discovery XL using the Orbitrap analyser (FTMS mode) at a nominal resolution of 7500. The average spectrum was processed with the software MagTran[90] for charge state deconvolution.

Determination of *Mt*IMPDH quaternary structure

Gel filtration chromatography was performed on a Superdex 200 (HR 10/30) column pre-equilibrated with buffer A, and containing 200 mM KCl or 200 mM NaCl, at a flow rate of 0.4 mL min^{-1}, as described elsewhere,[91] and homogeneous *Mt*IMPDH was loaded on the column at different concentrations (0.2, 0.6 and 1 mg ml^{-1}). In addition, cross-linking studies were performed to probe for the quaternary structure of the *Mt*IMPDH employing the method described by Fadouloglou *et al*.,[92] using crystallization supports with 120 µL of 25% (v/v) glutaraldehyde acidified with HCl in the reservoir. A siliconized coverslip was used to seal the reservoir, containing a 15 µL drop of protein suspension (0.6 mg mL^{-1} homogeneous recombinant *Mt*IMPDH in buffer A without M^+, or containing either 200 mM KCl or 200 mM NaCl). The plates were incubated at 30 C° for different time intervals and protein drops were subsequently analyzed by 12% SDS-PAGE.

Multiple sequence alignment

The amino acid sequences of the following IMPDH proteins, whose three-dimensional structures were solved, were included in the alignment: *P. aeruginosa* (WP_003124121.1)*, C. parvum* (XP_625342.1), *B. burgdorferi* (ACO38285.1), *H. sapiens II* (NP_000875.2), and *T. foetus* (AAB01581.1). Multiple amino acid sequence alignment was performed by CLUSTALW,[93] using the Gonnet matrix for amino acids substitutions and considering gap penalties, to recognize essential residues for nucleotide substrate(s) binding as well as to identify structural divergences which can be exploited to develop bacterial-specific inhibitors. For alignment improvement, 45, 9, 12, 10, 30 and 10 amino acids residues were removed from the *M. tuberculosis*, *P. aeruginosa*, *C. parvum*, *B. burgdorferi*, *H. sapiens II* and *T. foetus* IMPDHs, respectively.

Enzyme activity assays

The standard enzyme activity assay was performed at 37 °C and the buffer, if not stated otherwise, contained 50 mM Tris pH 8.5, 1 mM DTT and 200 mM KCl (500 µL final volume), as described by Usha *et al*.,[41] with minimal modifications (no EDTA was added to assay mixture). KCl, NaCl, RbCl, LiCl, CsCl and NH_4Cl were used as sources of the monovalent cations, and $MgCl_2$ and $CaCl_2$ as the divalent cations. The reaction was initiated by the addition of recombinant *Mt*IMPDH, and the production of NADH was monitored spectrophotometrically at 340 nm (ε_{340nm} = 6.22 $mM^{-1}cm^{-1}$) and corrected for non-catalyzed chemical reactions in the absence of *Mt*IMPDH. The production of APADH (reduced form of acetylpyridine adenine dinucleotide) was monitored at 363 nm (ε_{363nm} = 9.1 $mM^{-1}cm^{-1}$) and the standard oxidation-reduction potentials for NAD^+ and $APAD^+$ (oxidized form of acetylpyridine adenine dinucleotide) are -0.320 V and -0.258 V, respectively.[60] One unit of *Mt*IMPDH is defined as the amount of enzyme necessary to convert 1 µmol of substrate into product per min, in an optical path of 1 cm.

Steady-state kinetics

Determination of the apparent steady-state kinetic parameters were evaluated at varying concentrations of IMP (0.04 –1 mM) and fixed-saturating concentration of NAD^+ (3 mM), and at varying concentrations of NAD^+ (0.3–10 mM) and fixed-saturating level of IMP (1 mM), under standard assay conditions. The enzyme specificity for NAD^+ was evaluated measuring the enzymatic reaction in the presence of varying concentrations of

$NADP^+$ (0.8–20 mM) or $APAD^+$ (0.3–8 mM), at fixed-saturating concentration of IMP (1 mM). To assess the effect of monovalent cations on *Mt*IMPDH activity, initial velocity parameters were calculated as a function of different concentrations of Li^+, Na^+, K^+, NH_4^+, Rb^+ and Cs^+, at saturating concentrations of IMP (1 mM) and NAD^+ (3 mM). The dependence of the apparent kinetic constants for IMP and NAD^+ were also investigated varying the concentrations of these substrates in the presence of K^+, NH_4^+ or Rb^+, at saturating concentration (200 mM).

Additionally, initial velocity studies were carried out to determine the true steady-state kinetic parameters and the intersecting initial velocity patterns. For these experiments, the role of K^+ was regarded as an essential monovalent cation and the concentrations of two substrates were varied while maintaining the third substrate at a fixed-saturating concentration. Of the two different substrates, the concentration of one was varied whereas the second was maintained at different fixed concentrations.[19,74,76,94,95] The experimental conditions were as follows: i) varying NAD^+ concentrations (0.3–3 mM), fixed saturating level of IMP (2 mM) and fixed-varied K^+ concentrations (30, 66, 102, 198 and 240 mM); ii) varying NAD^+ concentrations (0.3–3 mM), fixed saturating level of K^+ (240 mM) and fixed-varied IMP concentrations (0.07, 0.1, 0.3, 0.5 and 1 mM); iii) varying K^+ concentrations (30–300 mM), fixed saturating level of IMP (2 mM) and fixed-varied NAD^+ concentrations (0.3, 0.8, 1.5, 2, 3 and 4 mM); and iv) varying K^+ concentrations (30–300 mM), fixed saturating level of NAD^+ (3 mM) and fixed-varied IMP concentrations (0.08, 0.1, 0.24, 0.5 and 1 mM).

Product inhibition kinetics

Product inhibition patterns were examined by measuring initial rates at varying concentrations of one substrate (IMP, NAD^+ or K^+), fixed non-saturating concentration of the co-substrate, and fixed-varying levels of products (either XMP or NADH).[59] Inhibition by monovalent cations were performed at varying concentrations of K^+, fixed non-saturating concentrations of both IMP and NAD^+, and at fixed-varied concentrations of Na^+ (0, 80, 160 and 240 mM) and Li^+ (0, 80, 120 and 160 mM). Inhibition studies were also carried out as a function of IMP and NAD^+ concentrations, in the presence of different fixed GMP or GTP concentrations (0, 200, 300, 400, 600 and 800 μM).

Kinetic parameters were also analyzed as a function of IMP and NAD^+ concentrations, at saturating concentrations of the co-substrates, in the absence or presence of a fixed concentration of AMP, ATP, UTP and CTP (500 μM) to verify whether these nucleotides have any effect on the kinetic properties of *Mt*IMPDH.

pH-rate profiles

Initial velocities measurements were carried out with increasing amounts of one substrate (IMP, NAD^+ or K^+) and saturating levels of the other two co-substrates, in 100 mM 2-(*N*-morpholino)-ethanesulfonic acid (MES)/Hepes/2-(*N*-cyclohexylamino)-ethanesulfonic acid (CHES) buffer mixture, over the following pH values: 7.0, 7.5, 8.0, 8.5, 9.0, 9.5 and 10.0, at 37 °C.[79] Prior to performing pH-rate studies, *Mt*IMPDH was incubated at the pH values cited above and assayed under standard conditions to ensure enzyme stability at the experimental pH values over the course of reaction.

Energy of activation

The energy of the *Mt*IMPDH-catalyzed chemical reaction was determined using saturating concentrations of IMP (2 mM) and NAD^+ (3 mM), in the standard activity assay, at temperatures ranging from 288 to 308 K. *Mt*IMPDH was incubated for several minutes at all temperatures tested and assayed under standard conditions to ensure enzyme stability.[85]

Data analysis

Initial velocity data and their respective errors were obtained by fitting the data to the appropriate equations by using the nonlinear regression function of SigmaPlot 9.0 2004 (SPSS, Inc.). Hyperbolic saturation curves were fitted by nonlinear regression analysis to the Michaelis-Menten equation,[96] Eq. (1), in which v is the initial velocity, V_{max} is the maximal rate, [S] is the substrate concentration, and K_m is the Michaelis-Menten constant. The substrate inhibition constant (K_i) was calculated using the substrate inhibition equation,[97] Eq. (2), in which K_i represents the dissociation constant for the inhibitory complex, and the remaining variables are as for Eq. (1). Sigmoidal curves were fitted to Eq. (3), where $K_{0.5}$ is a constant correlated to K_m, but also contains terms related to the effect of substrate occupancy at one site on the substrate affinity of other sites, and n is the Hill coefficient (related to the cooperative index):[61]

$$v = \frac{V_{max}[S]}{K_m + [S]} \quad \text{Eq. (1)}$$

$$v = \frac{V_{max}[S]}{K_m + [S] + \frac{[S]^2}{K_i}} \quad \text{Eq. (2)}$$

$$v = \frac{V_{max}[S]^n}{K_{0.5}^n + [S]^n} \quad \text{Eq. (3)}$$

Intersecting initial velocity patterns where fitted to Eq. (4), which describes a mechanism involving ternary complex formation and a sequential mechanism, where v is the initial velocity, V_{max} is the maximal initial velocity, [A] and [B] are the concentrations of IMP, NAD^+ or K^+, K_A and K_B are their respective Michaelis constants, and K_{ia} is the dissociation constant for enzyme-substrate A binary complex formation. In Eq. (4), A and B refer to substrates K^+ and NAD^+, respectively, when IMP was the fixed substrate. When K^+ was fixed at saturating concentration, A refers to IMP and B to NAD^+. Similarly, when NAD^+ was the fixed substrate, A refers to IMP and B to K^+.[76]

$$v = \frac{V_{max}[A][B]}{K_{ia}K_B + K_A[B] + K_B[A] + [A][B]} \quad \text{Eq. (4)}$$

Inhibition measurements were analyzed by fitting the data to competitive (Eq. (5)), noncompetitive (Eq. (6)) and uncompetitive (Eq. (7)) equations, where [I] is the inhibitor concentration, K_{is} is the dissociation constant for the binary EI complex and K_{ii} is the dissociation constant for the ternary ESI complex:[59,98]

$$v = \frac{V_{max}[S]}{[S] + K_m\left(1 + \frac{[I]}{K_{is}}\right)} \quad \text{Eq. (5)}$$

$$v = \frac{V_{max}[S]}{[S]\left(1+\frac{[I]}{K_{ii}}\right)+K_m\left(1+\frac{[I]}{K_{is}}\right)} \quad \text{Eq. (6)}$$

$$v = \frac{V_{max}[S]}{[S]\left(1+\frac{[I]}{K_{ii}}\right)+K_m} \quad \text{Eq. (7)}$$

Data for pH-rate profiles were fitted to Eq. (8) and (9), where y represents the kinetic parameter (k_{cat} or k_{cat}/K_m), C is the pH-independent value of y, H is the proton concentration, and K_a and K_b are, respectively, the apparent acid and base dissociation constants for ionizing groups.[79]

$$\log y = \log\left(\frac{C}{1+\frac{H}{K_a}}\right) \quad \text{Eq. (8)}$$

$$\log y = \log\left(\frac{C}{1+\frac{H}{K_a}+\frac{K_b}{H}}\right) \quad \text{Eq. (9)}$$

The data for temperature effects were fitted to Eq. (10), where k is the maximal reaction rate, E_a is the energy of activation, which was calculated from the slope ($-E_a/R$) of the Arrhenius plot, T is the temperature in Kelvin, R is the gas constant (8.314 J $mol^{-1}K^{-1}$) and A is a pre-exponential factor that correlates collision frequency and the probability of the reaction occurring when reactant molecules collide.[85]

$$\log k = -\left(\frac{E_a}{2.3R}\right)\left(\frac{1}{T}\right)+\log A \quad \text{Eq. (10)}$$

Acknowledgements

This work was supported by funds awarded by Decit/SCTIE/MS-MCT-CNPq-FNDCT-CAPES to National Institute of Science and Technology on Tuberculosis (INCT-TB) to D.S.S. and L.A.B. L.A.B. and D.S.S. also acknowledge financial support awarded by FAPERGS-CNPq-PRONEX-2009. L.A.B. (CNPq, 520182/99-5) and D.S.S. (CNPq, 304051/1975-06) are Research Career Awardees of the National Research Council of Brazil (CNPq). D.C.R. was the recipient of a PhD student scholarship awarded by CNPq.

References

1 World Health Organization, 2013. Global tuberculosis control: WHO report 2013. WHO/HTM/TB/2013.11.

2 E. M. Zager and R. McNerney, *BMC Infect. Dis.*, 2008, **8**, DOI: 10.1186/1471-2334/8/10.

3 M. Jassal and W. R. Bishai, *Lancet Infect. Dis*., 2009, **9**, 19-30.

4 E. S. Guy and A. Mallampalli, *Ther. Adv. Respir. Dis*., 2008, **2**, 401-408.

5 A. Zumla, P. Nahid and S. T. Cole, *Nat. Rev. Drug Discovery*, 2013, **12**, 388-404.

6 C. Sala and R. C. Hartkoorn, *Future Microbiol*., 2011, **6**, 617-633.

7 S. T. Cole, R. Brosch, J. Parkhill, T. Garnier, C. Churcher, D. Harris, S. V. Gordon, K. Eiglmeier, S. Gas, C. E. Barry, F. Tekaia, K. Badcock, D. Basham, D. Brown, T. Chillingworth, R. Connor, R. Davies, K. Devlin, T. Feltwell, S. Gentles, N. Hamlin, S. Holroyd, T. Hornsby, K. Jagels, A. Krogh, J. McLean, S. Moule, L. Murphy, K. Oliver, J. Osborne, M. A. Quail, M. A. Rajandream, J. Rogers, S. Rutter, K. Seeger, J. Skelton, R. Squares, S. Squares, J. E. Sulston, K. Taylor, S. Whitehead and B. G. Barrell, *Nature*, 1998, **393**, 537-544.

8 R. G. Ducati, L. A. Basso and D. S. Santos, *Curr. Drug Targets*, 2007, **8**, 423-435.

9 L. Hedstrom and C. C. Wang, *Biochemistry*, 1990, **29**, 849-854.

10 E. De Clercq, *Adv Virus. Res*., 1993, **42**, 1-55.

11 A. C. Allison and E. M. Eugui, *Immunopharmacology*, 2000, **47**, 85-118.

12 M. D. Sintchak and E. Nimmesgern, *Immunopharmacology*, 2000, **47**, 163-184.

13 Q. Shu and V. Nair, *Antiviral Chem. Chemother.*, 2007, **18**, 245-258.

14 Q. Shu and V. Nair, *Med. Res. Rev.*, 2008, **28**, 219-232.

15 L. Hedstrom, G. Liechti, J. B. Goldberg and D. R. Gollapalli, *Curr. Med. Chem.*, 2011, **18**, 1909-1918.

16 L. Hedstrom, *Chem. Rev.*, 2009, **109**, 2903-2928.

17 Y. Natsumeda, S. Ohno, H. Kawasaki, Y. Konno, G. Weber and K. Suzuki, *J. Biol. Chem.*, 1990, **265**, 5292-5295.

18 X. Zhou, M. Cahoon, P. Rosa and L. Hedstrom, *J. Biol. Chem.*, 1997, **272**, 21977-21981.

19 B. Xiang, J. C. Taylor and G. D. Markham, *J. Biol. Chem.*, 1996, **271**, 1435-1440.

20 J. A. Digits and L. Hedstrom, *Biochemistry*, 1999, **38**, 2295-2306.

21 M. D. Sintchak, M. A. Fleming, O. Futer, S. A. Raybuck, S. P. Chambers, P. R. Caron, M. A. Murcko and K. P. Wilson, *Cell*, 1996, **85**, 921-930.

22 F. G. Whitby, H. Luecke, P. Kuhn, J. R. Somoza, J. A. Huete-Perez, J. D. Phillips, C. P. Hill, R. J. Fletterick and C. C. Wang, *Biochemistry*, 1997, **36**, 10666-10674.

23 E. Nimmesgern, J. Black, O. Futer, J. R. Fulghum. S. P. Chambers, C. L. Brummel, S. A. Raybuck and M. D. Sintchak, *Protein Expression Purif.*, 1999, **17**, 282-289.

24 R. Zhang, G. Evans, F. J. Rotella, E. M. Westbrook, D. Beno, E. Huberman, A. Joachimiak and F. R. Collart, *Biochemistry*, 1999, **38**, 4691-4700.

25 K. M. Kerr and L. Hedstrom, *Biochemistry*, 1997, **36**, 13365-13373.

26 K. M. Kerr, M. Cahoon, D. A. Bosco and L. Hedstrom, *Arch. Biochem. Biophys.*, 2000, **375**, 131-137.

27 E. Nimmesgern, T. Fox, M. A. Fleming and J. A. Thomson, *J. Biol. Chem.,* 1996, **271**, 19421-19427.

28 L. Gan, G. A. Petsko and L. Hedstrom, *Biochemistry*, 2002, **41**, 13309-13317.

29 W. Wang and L. Hedstrom, *Biochemistry*, 1997, **36**, 8479-8483.

30 B. Xiang and G. D. Markham, *Arch. Biochem. Biophys.*, 1997, **348**, 378-382.

31 T. V. Riera, W. Wang, H. R. Josephine and L. Hedstrom, *Biochemistry*, 2008, **47**, 8689-8696.

32 R. Zhang, G. Evans, F. Rotella, E. Westbrook, E. Huberman, A. Joachimiak and F. R. Collart, *Curr. Med. Chem*., 1999, **6**, 537-543.

33 J. A. Digits and L. Hedstrom, *Biochemistry*, 2000, **39**, 1771-1777.

34 C. R. Johnson, S. K. Gorla, M. Kavitha, M. Zhang, X. Liu, B. Striepen, J. R. Mead, G. D. Cuny and L. Hedstrom, *Bioorg. Med. Chem. Lett*., 2013, **23**, 1004-1007.

35 S. K. Gorla, M. Kavitha, M. Zhang, J. E. W. Chin, X. Liu, B. Striepen, M. Makowska-Grzyska, Y. Kim, A. Joachimiak, L. Hedstrom and G. D. Cuny, *J. Med. Chem.*, 2013, **56**, 4028-4043.

36 L. Hedstrom, L. Gan, Y. G. Schlippe, T. Riera and M. Seyedsayamdost, *Nucleic Acids Res. Suppl*., 2003, **3**, 97-98.

37 D. R. Gollapalli, I. S. MacPherson, G. Liechti, S. K. Gorla, J. B. Goldberg and L. Hedstrom, *Cell Press Chemistry & Biology*, 2010, **17**, 1084-1091.

38 L. Chen, D. J. Wilson, Y. Xu, C. C. Aldrich, K. Felczak, Y. Y. Sham and K. W. Pankiewicz, *J. Med. Chem*., 2010, **53**, 4768-4778.

39 J. A. Digits and L. Hedstrom, *Biochemistry*, 1999, **38**, 15388-15397.

40 V. Usha, J. V. Hobrath, S. S. Gurcha, R. C. Reynolds and G. S. Besra, *PLoS One*, 2012, **7**, e33886.

41 V. Usha, S. S. Gurcha, A. L. Lovering, A. J. Lloyd, A. Papaemmanouil, R. C. Reynolds and G. S. Besra, *Microbiology*, 2011, **157**, 290-299.

42 C. M. Sassetti, D. H. Boyd and E. J. Rubin, *Mol. Microbiol.*, 2003, **48**, 77-84.

43 M. A. DeJesus, Y. J. Zhang, C. M. Sassetti, E. J. Rubin, J. C. Sacchettini and T. R. Ioerger, *Bioinformatic*, 2013, **29**, 695-703.

44 F. Dobie, A. Berg, J. M. Boitz and A. Jardim, *Mol. Biochem. Parasitol.*, 2007, **152**, 11-21.

45 M. C. Pinna, A. Salis, M. Monduzzi and B. W. Ninham, *J. Phys. Chem. B*, 2005, **109**, 5406-5408.

46 D. N. Okamoto, M. Y. Kondo, J. A. N. Santos, S. Nakajima, K. Hiraga, K. Oda, M. A. Juliano, L. Juliano and I. E. Gouvea, *Biochim. Biophys. Acta*, 2009, **1794**, 367-373.

47 R. L. Baldwin, *Biophys. J.*, 1996, **71**, 2056-2063.

48 M. M. Bradford, R. A. Mcroire and W. L. Williams, *Anal. Biochem.*, 1976, **72**, 248-254.

49 H. J. Gilbert, C. R. Lowe and W. T. Drabble, *Biochem. J.,* 1979, **183**, 481-494.

50 Y. Ji, J. Gu, A. M. Makhov, J. D. Griffith and B. S. Mitchell, *J. Biol. Chem.*, 2006, **281**, 206-212.

51 E. Heyde and J. F. Morrison, *Biochim. Biophys. Acta*, 1976, **429**, 635-644.

52 V. A. Rao, S. M. Shepherd, R. Owen and W. N. Hunter, *Sect. F: Struct. Biol. Cryst. Commun*., 2013, **F69**, 243-247

53 I. S. MacPherson, S. Kirubakaran, S. K. Gorla, T. V. Riera, J. A. D'Aquino, M. Zhang, G. D. Cuny and L. Hedstrom, *J. Am. Chem. Soc.*, 2013, **132**, 1230-1.

54 F. M. McMillan, M. Cahoon, A. White, L. Hedstrom, G. A. Petsko and D. Ringe, *Biochemistry*, 2000, **39**, 4533-4542.

55 T. D. Colby, K. Vanderveen, M. D. Strickler, G. D. Markham and B. M. Goldstein, *Proc. Natl. Acad. Sci*., 1999, **96**, 3531-3536.

56 G. L. Prosise, J. Z. Wu and H. Luecke, *J. Biol. Chem.*, 2002, **277**, 50654-50659.

57 G. L. Prosise and H. Luecke, *J. Mol. Biol.,* 2003, **326**, 517-527.

58 N. N. Umejiego, C. Li, T. Riera, L. Hedstrom and B. Striepen, *J. Biol. Chem*., 2004, **279**, 40320-40327.

59 P. F. Cook and W. W. Cleland, in *Enzyme Kinetics and Mechanism*, Garland Science Publishing, New York, 2007, ch. 6, pp. 121-204.

60 J. D. Hermes, S. W. Morrical, M. H. O'Leary and W. W. Cleland, *Biochemistry*, 1984, **23**, 5479-5488.

61 R. A. Copeland, in *Enzymes: A Practical Introduction to Structure, Mechanism, and Data Analysis*, Wiley-VCH, New York, 2000, ch. 12, pp. 367-384.

62 F. J. Bruzzese and P. R. Connelly, *Biochemistry*, 1997, **36**, 10428-10438.

63 P. R. Lambden and W. T. Drabble, *Biochem. J.*, 1973, **133**, 607-608.

64 L. Hedstrom and L. Gan, *Curr. Opin. Chem. Biol.*, 2006, **10**, 520-525.

65 J. P. Glusker, *Adv Protein Chem.,* 1991, **42**, 1-76.

66 J. F. Kachmar and P. D. Boyer, *J. Biol. Chem*., 1953, **200**, 669–682.

67 M. J. Page and E. Di Cera, *Physiol. Rev*., 2006, **86**, 1049-1092.

68 S. H. E. Kaufmann, *Nat. Rev. Immunol*., 2001, **1**, 20-30.

69 J. D. Ernst*, Nat. Rev. Immunol*., 2012, **12**, 581-591.

70 D. Wagner, J. Maser, B. Lai, Z. Cai, C. E. Barry III, K. H. zu Bentrup, D. G. Russell and L. E. Bermudez, *J. Immunol.*, 2005, **174**, 1491-1500.

71 S. Rana, N. Pozzi, L. A. Pelc and E. Di Cera, *PNAS*, 2011, **108**, 5221-5225.

72 G. D. Markham, C. L. Bock and C. Schalk-Hihi, *Biochemistry*, 1999, **38**, 4433-4440.

73 T. V. Riera, L. Zheng, H. R. Josephine, D. Min, W. Yang and L. Hedstrom, *Biochemistry*, 2011, **50**, 8508-8518.

74 E. Heyde, A. Nagabhushanam, M. Vonarx and J. F. Morrison, *Biochim. Biophys. Acta*, 1976, **429**, 645-660.

75 O. Futer, M. D. Sintchak, P. R. Caron, E. Nimmesgern, M. T. DeCenzo, D. J. Livingston and S. A. Raybuck, *Biochim. Biophys. Acta*, 2002, **1594**, 27-39.

76 P. F. Cook and W. W. Cleland, in *Enzyme Kinetics and Mechanism*, Garland Science Publishing, New York, 2007, ch. 5, pp. 59-120.

77 R. Verham, T. D. Meek, L. Hedstrom and C. C. Wang, *Mol. Biochem. Parasitol*., 1987, **24**, 1-12.

78 S. F. Carr, E. Papp, J. C. Wu and Y. Natsumeda, *J. Biol. Chem.,* 1993, **268**, 27286-27290.

79 P. F. Cook and W. W. Cleland, in *Enzyme Kinetics and Mechanism*, Garland Science Publishing, New York, 2007, ch. 10, pp. 325-366.

80 G. Bulaj, T. Kortemme and D. P. Goldenberg, *Biochemistry*, 1998, **37**, 8965-8972.

81 L. C. Antonino, K. Straub and J. C. Wu, *Biochemistry*, 1994, **33**, 1760-1765.

82 G. H. Peters, T. M. Frimurer and O. H. Olsen, *Biochemistry*, 1998, **37**, 5383-5393.

83 R. A. Copeland, in *Enzymes: A Practical Introduction to Structure, Mechanism, and Data Analysis*, Wiley-VCH, New York, 2000, ch. 7, pp. 241-248.

84 N. M. Goodey and S. J. Benkovic, *Nat. Chem. Biol.*, 2008, **4**, 474-482.

85 I. H. Segel, in *Enzyme kinetics, behavior and analysis of rapid equilibrium and steady-state enzyme systems*, John Wiley & Sons, Inc., New York, 1975, ch. 11, pp. 926-934.

86 K. Gunasekaran, B. Ma and R. Nussinov, *Proteins*, 2004, **57**, 433-443.

87 U. K. Laemmli, *Nature*, 1970, **227**, 680-685.

88 Tuberculist *Mycobacterium tuberculosis* Database. http://tuberculist.epfl.ch/.

89 J. Sambrook, D. W. Russel, in *Molecular Cloning: A Laboratory Manual*, Spring Harbor Laboratory Press, New York, 2001, vol. 3, ch. 15, pp. 15.14-15.60.

90 Z. Zhang and A. G. Marshall, *J. Am. Soc. Mass Spectrom.*, 1998, **9**, 225-233.

91 D. C. Rostirolla, A. Breda, L. A. Rosado, M. S. Palma, L. A. Basso and D. S. Santos, *Arch. Biochem. Biophys.*, 2011, **505**, 202-212.

92 V. E. Fadouloglou, M. Kokkinidis and N. M. Glykos, *Anal. Biochem.*, 2008, **373**, 404-406.

93 J. D. Thompson, D. G. Higgins, T. J. Gibson, *Nucleic Acids Res.*, 1994, **22**, 4673-4680.

94 C. Frieden, *J. Biol. Chem.*, 1959, **234**, 2891-2896.

95 J. Y. Bhat, B. G. Shastri and H. Balaram, *Biochem. J.*, 2008, **409**, 263-273.

96 R. A. Copeland, in *Evaluation of Enzyme Inhibitors in Drug Discovery: A Guide for Medicinal Chemists and Pharmacologists*, John Wiley & Sons, Inc., New Jersey, 2005, ch. 2, pp. 21-47.

97 I. J. MacRae and I. H. Segel, *Arch. Biochem. Biophys.*, 1999, **361**, 277-282.

98 R. A. Copeland, in *Evaluation of Enzyme Inhibitors in Drug Discovery: A Guide for Medicinal Chemists and Pharmacologists*, John Wiley & Sons, Inc., New Jersey, 2005, ch. 3, pp. 48-81.

Figure legends

Figure 1: Chemical reaction catalyzed by IMPDH in the presence of a monovalent cation (M^+).

Figure 2: *Mt*IMPDH quaternary structure assignment by glutaraldehyde cross-linking experiments. Incubation times (in minutes) are shown at the bottom of each lane. Lane 1, Page Ruler Marker (Fermentas); Lane 2, *Mt*IMPDH monomer (*ca.* 55 kDa); Lane 3, 4 and 5, *Mt*IMPDH oligomers (*ca.* 220 kDa).

Figure 3: Amino acid sequence alignment of *M. tuberculosis* IMPDH (NCBI reference: NP_217928.1) with enzymes from *P. aeruginosa* (NCBI reference: WP_003124121.1), *C. parvum* (NCBI reference: XP_625342.1), *B. burgdorferi* (GenBank: ACO38285.1), *H. sapiens II* (NCBI reference: NP_000875.2) and *T. foetus* (GenBank: AAB01581.1), using the program CLUSTALW.[93] Residues involved in interactions with IMP, including the catalytic cysteine, are shaded in gray. Two conserved residues on the mobile flap are boxed by a dashed line. The residues involved in NAD/MPA binding in the human enzyme but divergent in the microbial IMPDHs were boxed by a solid line, and the black arrow indicates the conserved residue that interacts with MPA. Amino acid residues were numbered after removing 45 N-terminal amino acids from the polypeptide sequence of *Mt*IMPDH.

Figure 4: Apparent steady-state kinetic parameters measured under standard assay conditions. (A) Specific activity (U mg^{-1}) versus [NAD^+] (μM) at fixed concentration of IMP (1 mM); (B) Specific activity (U mg^{-1}) versus [$APAD^+$] (μM) at fixed concentration of IMP (1 mM). Data were analyzed using Eq. (2).

Figure 5: Velocity as a function of IMP concentration. (A) Specific activity (U mg^{-1}) versus [IMP] (μM) at fixed concentration of NAD^+ (3 mM), when data were fitted to the Hill equation. (B) Representative plot for specific activity (U mg^{-1}) versus [IMP] (μM) at fixed concentration of NAD^+ (3 mM), when data were fitted to the Michaelis-Menten equation. The insets of (A) and (B) display the calculated residual values plotted against IMP concentration using Eq. (3) and (1), respectively.

Figure 6: Intersecting initial velocity patterns for *Mt*IMPDH. (A) NAD^+ as the variable substrate (0.3–3 mM) at fixed saturating level of IMP (2 mM) and fixed-varied K^+ concentrations (30, 66, 102, 198 and 240 mM); (B) K^+ as the variable substrate (30–300 mM) at fixed saturating level of IMP (2 mM) and fixed-varied NAD^+ concentrations (0.3, 0.8, 1.5, 2, 3 and 4 mM). (C) NAD^+ as the variable substrate (0.3–3 mM) at fixed saturating level of K^+ (240 mM) and fixed-varied IMP concentrations (0.07, 0.1, 0.3, 0.5 and 1 mM); (D) K^+ as the variable substrate (30–300 mM) at fixed saturating level of NAD^+ (3 mM) and fixed-varied IMP concentrations (0.08, 0.1, 0.24, 0.5 and 1 mM).

Figure 7: Double-reciprocal plots for *Mt*IMPDH inhibition by GMP. (A) Specific activity^{-1} (mg U^{-1}) versus $[IMP]^{-1}$ (μM^{-1}) at fixed-varied concentrations of GMP; (B) Specific activity^{-1} (mg U^{-1}) versus $[NAD^+]^{-1}$ (μM^{-1}) at fixed-varied concentrations of GMP. Data were analyzed using Eq. (6) for (A) and Eq. (7) for (B).

Figure 8: pH-rate profiles for *Mt*IMPDH catalyzed reaction. (A) pH dependence of log k_{cat}; (B) pH dependence of log k_{cat}/K_{NAD+}. Experimental data were fitted to Eq. (8) and (9).

Figure 9: Temperature dependence of log k_{cat}. Saturating concentrations of IMP, NAD^+ and K^+ were employed to measure the maximum velocity as a function of temperature ranging from 288 to 308 K. Data were fitted to Eq. (10).